**MEASURING THE DISPERSION
OF LASER CAVITY MIRRORS USING
WHITE-LIGHT INTERFEROMETRY**

THESIS

Allison S. Goodspeed, Captain, USAF

AFIT/GAP/ENP/08-M06

**DEPARTMENT OF THE AIR FORCE
AIR UNIVERSITY**

AIR FORCE INSTITUTE OF TECHNOLOGY

Wright-Patterson Air Force Base, Ohio

MEASURING THE DISPERSION
OF LASER CAVITY MIRRORS USING
WHITE-LIGHT INTERFEROMETRY

THESIS

Presented to the Faculty

Department of Engineering Physics

Graduate School of Engineering and Management

Air Force Institute of Technology

Air University

Air Education and Training Command

In Partial Fulfillment of the Requirements for the

Degree of Master of Science

Allison S. Goodspeed, BS, MBA

Captain, USAF

March 2008

MEASURING THE DISPERSION
OF LASER CAVITY MIRRORS USING
WHITE-LIGHT INTERFEROMETRY

Allison S. Goodspeed, BS, MBA
Captain, USAF

Approved:

_____//signed//_____   _____
Matthew J. Bohn (Chairman)   Date

_____//signed//_____   _____
Robert L. Hengehold (Member)   Date

_____//signed//_____   _____
Robert G. Bedford (Member)   Date

AFIT/GAP/ENP/08-M06

ABSTRACT

      Terahertz radiation is an emerging field that has far reaching applications. There is a need for portable and affordable terahertz sources that may be used for detection of structural weaknesses in aerospace composites. One possibility for terahertz generation is a femtosecond Cr:LiSAF laser. However, controlling intracavity dispersion is necessary in order to get the ultrashort pulses needed to generate terahertz radiation. This research measures dispersion of the chirped femtosecond intracavity mirrors by employing white-light interferometry and explains the theory behind the curve-fitting process used to calculate dispersion. To compensate for the narrow reflectivity band of the mirrors, a CaF_2 (calcium fluoride) window was used to increase the number of spectral fringes in the interferogram. A cavity was designed using these mirrors and the Cr:LiSAF laser was successfully modelocked.

ACKNOWLEDGMENTS

I would like to express my sincerest appreciation to my faculty advisor, Lt Col Matthew J. Bohn, for his guidance and support throughout the course of this thesis effort. The insight and experience was really appreciated! I would also like to thank my sponsor, Dr. Robert Bedford, from the Air Force Research Laboratory for the support provided to me in this endeavor. Finally, I would like to thank Mr. Gregory Smith and Mr. Michael Ranft, the AFIT lab technicians, for their time and expertise.

<div align="right">Allison S. Goodspeed</div>

TABLE OF CONTENTS

LIST OF FIGURES

LIST OF TABLES

MEASURING THE DISPERSION OF LASER CAVITY MIRRORS USING WHITE-LIGHT INTERFEROMETRY

I. Introduction

Modelocked, diode-pumped Cr:LiSAF (chromium-doped lithium strontium aluminum fluoride) lasers offer a portable and affordable alternative to commercial Ti:Sapphire (titanium sapphire) laser systems. When modelocked, they are energy efficient and capable of producing femtosecond pulses (10^{-15} s = 1 fs) that can be used to generate terahertz radiation. In addition, Cr:LiSAF lasers can be used in detection devices to locate weaknesses in aerospace composites and to observe ultrafast processes such as a molecule undergoing a chemical reaction.

Controlling cavity dispersion is crucial to modelocking a laser. This research used white-light interferometry to measure dispersion in laser cavity mirrors. The dispersion results were then used to engineer a modelocked laser cavity with the goal of generating terahertz radiation.

Dispersion occurs when the phase velocity of a wave depends on its frequency. For optical fields, the angular frequency is $\omega = c/k_0$, where c is the speed of light in a vacuum and $k_0 = 2\pi/\lambda_0$. For a pulse, the phase velocity is

$v_p = w/k$, the group velocity is $1/v_g = \partial k/\partial \omega$, and the group-velocity dispersion is $GVD = \partial^2 k/\partial \omega^2$. The main concern of this paper is group-delay dispersion $GDD = GVD \times L$, which accounts for the length of dispersive media, L, and also applies to mirrors and laser cavities. It is commonly described in units of fs^2. Positive GDD causes a pulse to broaden temporally, making it difficult to achieve the desired effects of ultrashort pulses. This research focused on optical elements that contribute negative GDD and counteract pulse spreading.

This experiment is a continuation of the thesis work done by David Jones, a previous AFIT student [1]. The group delay dispersion of the optical components in the Cr:LiSAF laser cavity were measured using white-light interferometry. This information was used to analyze dispersion in the laser cavity. The goal was to create negative GDD, a condition for soliton-like modelocking. This concept is expanded in Appendix A. Derivation of the Non-Linear Schrödinger Equation. Characterization of the CW beam and modelocking the laser precede the goal of generating terahertz radiation.

Background

Reliable sources and detectors of terahertz radiation (T-rays) were hard to find until the 1990s. Now they are available on a limited basis, typically large systems for scientific research. In 2006, electrical engineer Daniel Mittleman, from Rice University's T-ray lab said: "The technology is very young. Terahertz is now where X-rays were in 1905 [2]."

T-rays can be used for detection in organic and inorganic materials, communication, and astronomy. They are capable of penetrating non-conducting materials like clothing and plastic, but not metal or water. Unlike X-rays, T-rays do not damage body tissue, so they are safe for medical imaging. When looking at tissue, T-rays are able to detect differences in density that make them useful for finding tumors.

T-rays have astronomical applications as well. The Herschel Space Observatory, a satellite due to launch in 2008, is the terahertz version of the Hubble telescope [2]. DOD interest includes non-destructive testing of aerospace composites, T-ray radar, and secure communications. Since many aircraft structures are built from composite materials, it is important to identify small cracks and delaminations. With a small, portable, T-ray source, this and many other applications would be possible.

Previous Work

All-solid-state laser systems became available over a decade ago. Since then, the use of tunable femtosecond lasers has grown to the point where they have become a fundamental tool in many areas of science, including physics, chemistry, and biology [3]. Materials scientists probe the dynamics of electrons in carbon nanotubes by carefully tuning a laser pulse's wavelength for time-resolved ultrafast spectroscopy. Physicists also use tunable ultrafast laser

sources to explore the specific responses of different nonlinear optical materials [3].

Cr:LiSAF lasers were first demonstrated in the 1990s by M. J. P. Dymott and A. I. Ferguson [4]. Their goal was to generate short pulses with a high repetition rate and high power. Their motivation was to create an all-solid-state alternative to the large Ti:Sapphire laser [5]. All-solid-state lasers are logistically simpler than gas lasers or dye lasers; and the Cr:LiSAF laser is a nice alternative to the Ti:Sapphire laser because it has a smaller footprint and an uncomplicated laser cavity.

A recently published experiment used spectral filters on flash lamp pumps to reduce waste heat in the laser crystal. The Centro de Lasers e Aplicacões in São Paulo, Brazil reported capabilities of 30 W average power at 851 nm, with 2 J pulses at 15 Hz. With a more restrictive filter, they showed average powers of 20 W but peak powers of 10kW at 30 Hz [6]. This group focused on increasing power from Cr:LiSAF lasers, not T-ray production.

Increasing continuous wave (CW) power is worthwhile, but short pulses inherently have high peak powers, so more can be done with a lower average power. The intensity of a CW laser, I_{CW}, is simply defined as

$$I_{CW} = \frac{Power}{Area}.$$

(1.1)

The intensity of a pulse, however, must consider the pulsewidth, τ_p, and the

time between pulses, τ_{RT}, which is derived from the cavity length, L, using

$$\tau_{RT} = \frac{1}{\nu} = \frac{2L}{c} , \qquad (1.2)$$

where ν is the pulse frequency, and c is the speed of light. Taking the unique

qualities of a pulse into consideration yields:

$$P_p = \frac{P_{CW} \times \tau_{RT}}{\tau_p} . \qquad (1.3)$$

Compared to τ_{RT}, τ_p is very short, so one can see in (1.3) that peak power can

be significant, even if the averaged CW power is unremarkable [7]. Modelocking

is the easiest way to get short pulses from a laser.

Modelocking can only be achieved if cavity dispersion is controlled.

Previous work on measuring dispersive media, both reflective and transmissive,

used white-light interferometry. That experimental technique is very different

than the work presented in this research. It used a compensated Michelson

interferometer that is later unbalanced with the addition of dispersive media. A

He-Ne laser is co-aligned with the collimated white-light beam, and the fringes

are sampled using a second detector. By linking this detector to a piezoelectric

translating stage, the movement of the delay arm is measured to sub-wavelength

accuracy. To find dispersion, a reference is first taken without the dispersive

media using a square-law detector that sees the intensity of the spatial fringes as

the delay arm is scanned. A second collection is taken with the dispersive

media, and then normalized using the reference data. The resulting plot contains the phase information. By fitting a fifth-degree polynomial to the curve, it is possible to discover the dispersive properties of the media with less than 4% error [8-10].

Research Objective

Modelocked lasing from this cavity depends on compensating for the positive GDD introduced by the Cr:LiSAF crystal. White-light interferometry was used to measure the amount of GDD contributed by mirrors in the cavity. Chapter 2 covers GDD in further detail.

This research furthered the development of a terahertz radiation source that is small, inexpensive, portable, and rugged. The concepts used in this system may be miniaturized, or expanded into a larger but still simple system. The applications of this technology are far reaching - including biomedical imaging, aerospace composite testing, airport security systems, and communications.

II. Theory

This section covers the Cr:LiSAF laser cavity design, including selection of the gain medium, necessary intracavity corrections, dispersion control, and modelocking. It also covers the mathematical theory supporting the use of a Michelson interferometer to measure GDD in the laser cavity mirrors. The MI theory is extended to explain the curve-fitting procedure used for data analysis. Finally, Grenouille FROG, another method of GDD measurement is described.

Cavity Design

The basic cavity design (Figure 1) has the following components: a polarizing beam splitter (PBS); two spherical mirrors (SM) (R = 99.9%); two planar mirrors; one with high reflectivity (99.9%); and one with lower reflectivity (99.0%) that acts as an output coupler (OC). A 3 mm long × 3 mm diameter Cr:LiSAF crystal with 5% doping lies between the two spherical mirrors. Two AlGaInP (aluminum gallium indium phosphide) diode lasers are aligned such that one is polarized vertically while one is polarized horizontally and are combined in a PBS. The combined beam passes through a lens (f = 5 cm), through the back of a spherical mirror, and focuses on the crystal. The lens focuses the beam so the volume of the cavity mode matches the gain volume of the crystal. To form a ring cavity the two planar mirrors are adjusted to reflect the beam from each spherical mirror onto the opposite planar mirror. The

spherical mirrors are adjusted so that the beam waist is halfway between the planar mirrors. In this configuration the CW beam propagates bi-directionally. However, when the laser is modelocked, unidirectional propagation is preferred. This effect is due to gain competition and the nonlinear loss mechanism induced via the Kerr lens. When a saturable absorber mirror (SAM) is introduced into the cavity, the beam path is linear (Figure 2).

The Cr:LiSAF crystal was selected because of its absorption and emission spectra (Figure 3). There is a broad absorption band centered near 650 nm and an emission spectrum centered near 840 nm. Semiconductor laser diodes, made with AlGaInP, operate at this peak absorption wavelength and are readily available at a relatively low cost. These diode lasers are the same lasers used in DVD burners. Their beam quality is excellent since burners require the beam to focus to a small spot size.
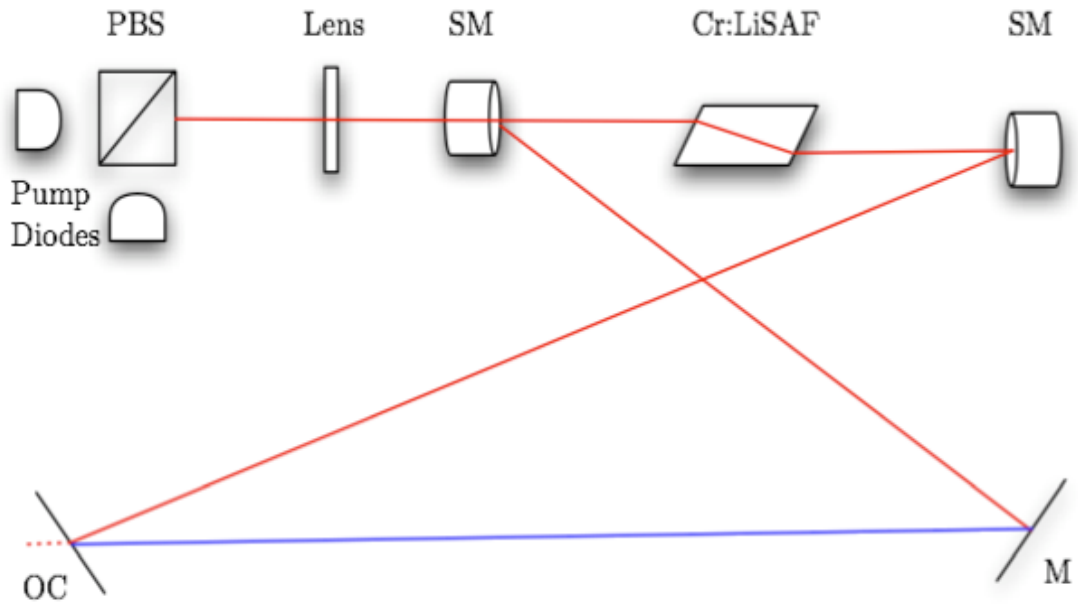
Figure 1. Cavity design and laser path for linear (red) and ring (red & blue)
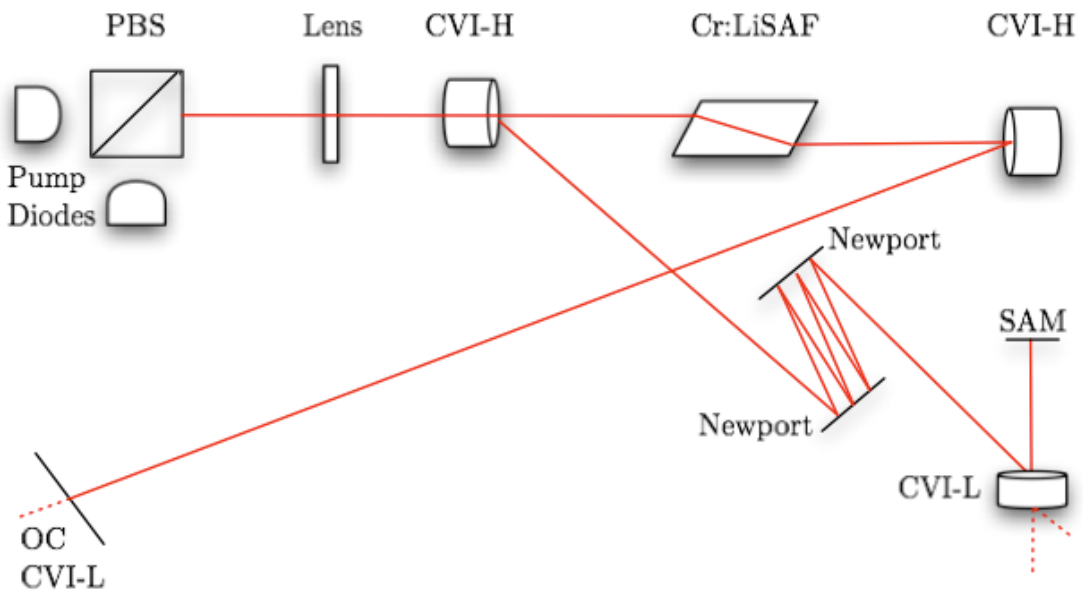
Figure 2. Linear cavity using SAM for passive modelocking

The emission spectrum of Cr:LiSAF is similar to the more common commercial Ti:Sapphire lasers, making it easy to find chirped mirrors, and other optical components. Cr:LiSAF is an excellent gain material with good energy storage and slope efficiency, which makes it ideal for use in pulsed lasers with high peak powers. So, using this crystal as the gain medium allows for an efficient, cost-effective device.
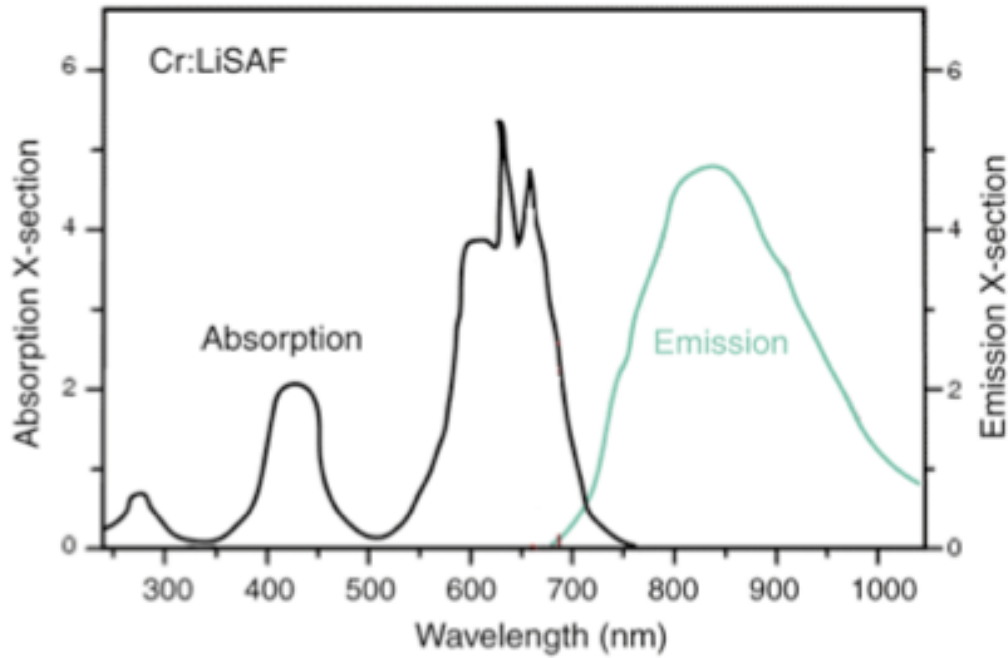
Figure 3. Cr:LiSAF absorption and emission spectra [11].

Cavity Correction

There are two types of correction needed in the cavity: astigmatism and GVD. Astigmatism is introduced into the beam as it passes through the Brewster's angle cut laser crystal. The vertical and horizontal planes of the beam follow different paths, resulting in an elliptically shaped beam hitting the

spherical mirrors. With a small angle of incidence, the spherical mirrors correct this astigmatism, restoring the beam to a circular cross-section.

GVD refers to a specific effect of an optical medium on a pulse of light. Pulse envelopes are made up of a number of frequency components, which are added together coherently. In a dispersive system, these frequency components travel at different velocities, so the initially short pulse may broaden [12]. Positive GVD slows the shorter wavelengths with respect to the longer wavelengths (Figure 4). This delay results in temporally broadened pulses.
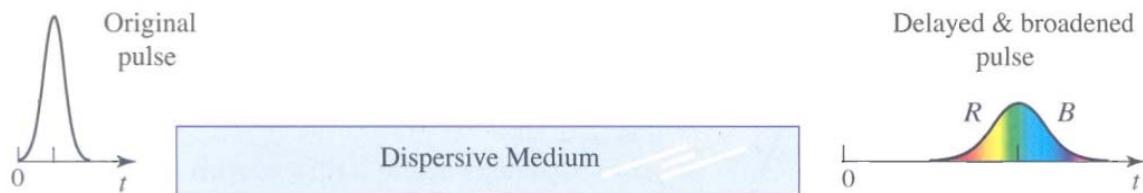
Figure 4. Positive GVD for a pulse in a dispersive medium [13].

The Sellmeier equation can be used to find the amount of dispersion in terms of wavelength for a given material. From Diels, GVD is 250 fs^2/cm for 2% doped Cr:LiSAF. In this 3 mm long 5% doped crystal, the GDD is 75 fs^2 [10]. In a linear cavity, the beam passes through the crystal twice, so the GDD doubles.

Chirped mirrors have special multilayer dielectric coatings with periodic spatial frequency. They reflect shorter wavelengths at the layers closest to the front surface, while allowing longer wavelengths to penetrate deeper layers before being reflected (Figure 5).

11
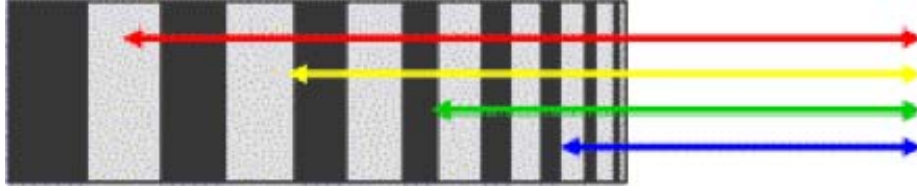
Figure 5. Operation principle of a chirped mirror. Long wavelengths penetrate deeper into the mirror structure and thus experience a delay [14].

This causes the delay of the longer wavelengths needed to create negative GDD. It counters the effect of the crystal and shortens the pulse. Chirped mirrors are mainly used inside Ti:Sapphire oscillators that produce pulses shorter than 30 fs [3]. The chirped mirrors in this experiment are optimized for femtosecond-pulsed laser systems. The advantage of chirped mirrors over other types of dispersion compensation is negative GDD over the whole bandwidth of femtosecond pulses. Assuming a Gaussian pulse, the negative GDD results in an ideal linear chirp [15].

Chirp is the name for a change in frequency within a pulse envelope. As a pulse propagates through the crystal, it undergoes self-phase modulation (SPM). This is a small non-linear effect where the pulse experiences a phase shift, and subsequent change in the frequency spectrum (Figure 6). The frequency either increases (up chirped) or decreases (down chirped) with time. An up chirped pulse is shown in Figure 7. SPM broadens the spectral bandwidth, and gives short pulses in the time domain via the Fourier transform, as there is an inverse relationship between bandwidth and temporal pulse length.
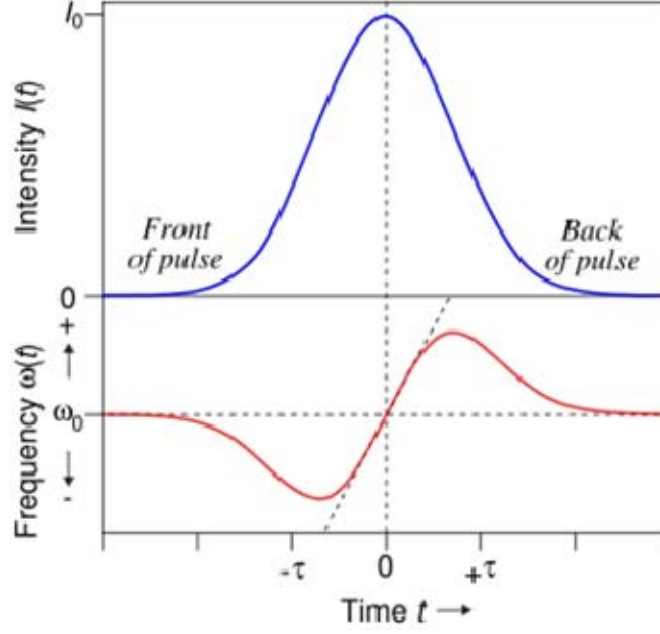
Figure 6. A pulse (top curve) propagating through a non-linear medium undergoes a self-frequency shift (bottom curve) due to SPM. The front of the pulse is shifted to lower frequencies, the back to higher frequencies. In the center of the pulse, the frequency shift is approximately linear [10].
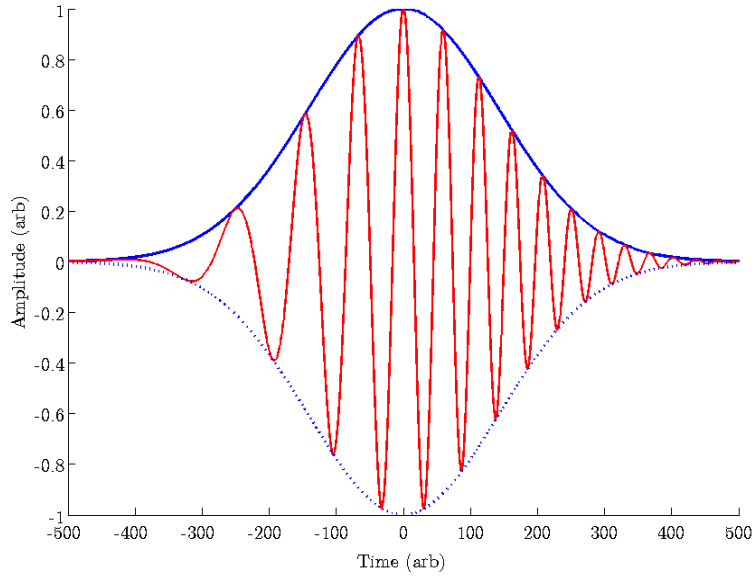
Figure 7. A positively chirped pulse in the time domain, resulting from SPM. In this figure, the amplitude is a Gaussian function. The phase is quadratic, resulting in an instantaneous frequency sweep.

13

Modelocking

The primary source for ultrashort optical pulses is the modelcked laser oscillator [12]. When many longitudinal modes of the laser cavity (~186,000 in this case) are modelocked and equally spaced in frequency they combine to generate short pulses. Another way to picture modelocking is a single pulse propagating around the laser cavity must have the same shape after one round trip; this is the definition of a soliton. Further discussion of the soliton solution may be found in Appendix A. Derivation of the Non-Linear Schrödinger Equation. The output of a modelocked laser is a train of pulses at an interval equal to the round-trip time of the cavity. This concept was introduced earlier with Equation (1.2) and (1.3). The shortest possible pulse duration is limited by the inverse gain bandwidth [7].

There are active and passive methods to achieve modelocked lasing. Active modelocking involves modulating the intracavity loss or phase, while passive modelocking involves using intracavity, intensity dependent, dispersion control elements that favor pulsed over CW operation. They cause cavity modes that are above threshold to have the same phase, and lock together [12]. This section will focus on the two passive methods for modelocking the Cr:LiSAF laser: the Kerr-lens effect and a saturable absorber mirror (SAM).

The Kerr effect occurs in non-linear crystals, where the index of refraction depends on beam intensity. Short pulses with high peak intensities are well

suited to induce the Kerr effect. As the intensity increases, so does the index; the crystal acts like a lens, focusing the beam (Figure 8).
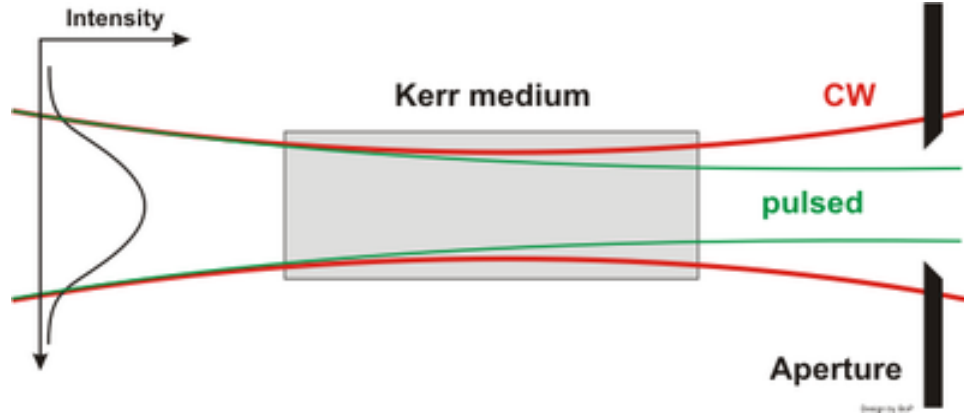
Figure 8. Kerr-lens modelocking principle [16].

When attempting to modelock a laser it is possible to take advantage of the Kerr-lens effect by inserting an aperture in the beam. If the laser is modelocked, the pulses have high peak intensity, and the Kerr effect causes the crystal to focus the beam. As the beam is focused, the waist shifts from its CW location to a different modelocked location. If an aperture is placed at the modelocked waist location, a pulse will experience less loss than a CW beam. By passing the pulses, the lens effect increases in the crystal and the pulse experiences more gain in each round-trip, driving the laser into pulsed modelocked operation.

The other passive modelocking element used in the Cr:LiSAF cavity is a SAM. A simple diagram is shown in Figure 9. Each SAM must be carefully

designed for a specific application. At the far side, there is a Bragg-mirror on a semiconductor wafer substrate. This is covered with an absorber layer and then a sophisticated top film system, which determines saturable loss [17]. At high intensities, the absorber is saturated and becomes transparent to pulses, allowing them to pass through to the Bragg-mirror, where they are reflected back into the cavity. At low intensities, the absorber is not saturated, and removes more of the incident energy from the cavity. This SAM loss mechanism results in phase locking that causes pulses in the cavity.
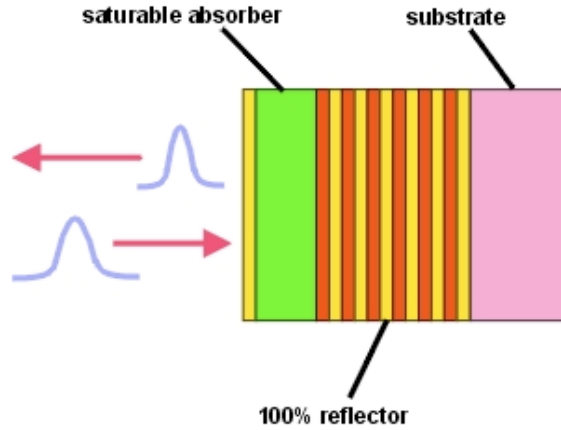
Figure 9. Saturable Absorber Mirror [17].

Modelocking with the Kerr effect and SAM can only be achieved if the positive GVD from the laser crystal and the positive chirp from SPM are corrected with negative GDD mirrors. White-light interferometry was used to measure GDD in these laser cavity mirrors.

White Light Interferometry

Cr:LiSAF introduces frequency-dependent positive dispersion into the laser cavity. This GDD is partially a result of the ultrafast SPM caused by the optical Kerr effect. Chirped dielectric mirrors with negative GDD balance the Kerr effect in broad bandwidth pulses. A standard Michelson interferometer and a white-light source can be used to measure the dispersive properties of both transmissive and reflective optical components. The goal is to measure the GDD of the mirrors used in the Cr:LiSAF laser cavity in order to determine if the net GVD is negative. This will provide the information needed to choose mirrors with the right amount of negative GDD in order to modelock the laser and generate terahertz radiation.

White Light

White light is the best choice to measure laser cavity mirrors because it mimics the broad bandwidth and short coherence length of femtosecond pulses. A Michelson interferometer uses a beam splitter and mirrors to create an interference fringe pattern. Fringes occur when two or more light waves yield a resulting irradiance that deviates from the sum of the component irradiances [18]. If two beams interfere and create fringes, they consist of nearly the same frequency. However, if the beams are both white light, which contains many frequencies, then the reds will interfere with only the reds, the blues with only the blues, etc., producing fringes as well.

17

As a quick review, here are some characteristics of white light, and how it lends itself to this application. White light is essentially incoherent, like sunlight -- unless one looks on a femtosecond time-scale. Its limited temporal coherence is very similar to ultrafast pulses. A white light source emits many wavelengths (temporal incoherence), and the phase of the light emitted from different regions of the source are not correlated (spatial incoherence). The coherence time, τ_0, is

$$\tau_0 = \frac{1}{\Delta\nu} = \frac{\lambda}{\nu|\Delta\lambda|}, \tag{2.1}$$

where

$$\Delta\lambda = \frac{\lambda^2}{c}\Delta\nu. \tag{2.2}$$

The longer the coherence time, the greater the temporal coherence of the source [16]. Another way to describe coherence time is the interval over which the light wave resembles a sinusoid. For white light, $\tau_0 \approx 10^{-14}$ s, which is very short compared to a standard He-Ne laser, where $\tau_0 \approx 10^{-3}$ s.

The coherence length, l_c, is

$$l_c = c\tau_0 = \frac{\lambda^2}{|\Delta\lambda|}. \tag{2.3}$$

Fringes can appear on the detector when the difference between the beam paths to each mirror is less than half the coherence length,

$$l_c \geq 2\left(l_2 - l_1\right). \tag{2.4}$$

Here, l_1 and l_2 are the distances from the beam splitter to each mirror,

18

respectively. Additionally, the total phase difference must be an integer multiple

of π, and less than the coherence length (2.4). For white light, $l_c \approx 2 \times 10^{-4}$ cm,

which is much shorter than a He-Ne laser, where $l_c \approx 3 \times 10^7$ cm.

Interference Theory

In this experiment, a white light source is directed into a Michelson

interferometer (Figure 10). When it reaches the beamsplitter, half of the light

passes straight through to the first mirror and half of the light is reflected 90° to

the second mirror. After reflection on the mirrors, the beamsplitter directs the

combined beams towards a detector. Where the reflected beams overlap,

interference fringes are expected when the path lengths are the same and they

meet the criteria described in the previous section.

The fringe visibility, V, can be described quantitatively as

$$V = \frac{I_{max} - I_{min}}{I_{max} + I_{min}}. \tag{2.5}$$

The intensities in (2.5) correspond to a maximum and adjacent minimum in the

fringe system. The greatest contrast between the dark and light fringes is when

V=1 [18]. Since the visibility depends on the delay between the beams, τ, it

can also be described to the first order as

$$V\left(\tau\right) = 1 - \frac{\tau}{\tau_0}, \tag{2.6}$$

when $\tau \leq \tau_0$, and zero otherwise [16]. Coherence time, τ_0, is defined in (2.1).
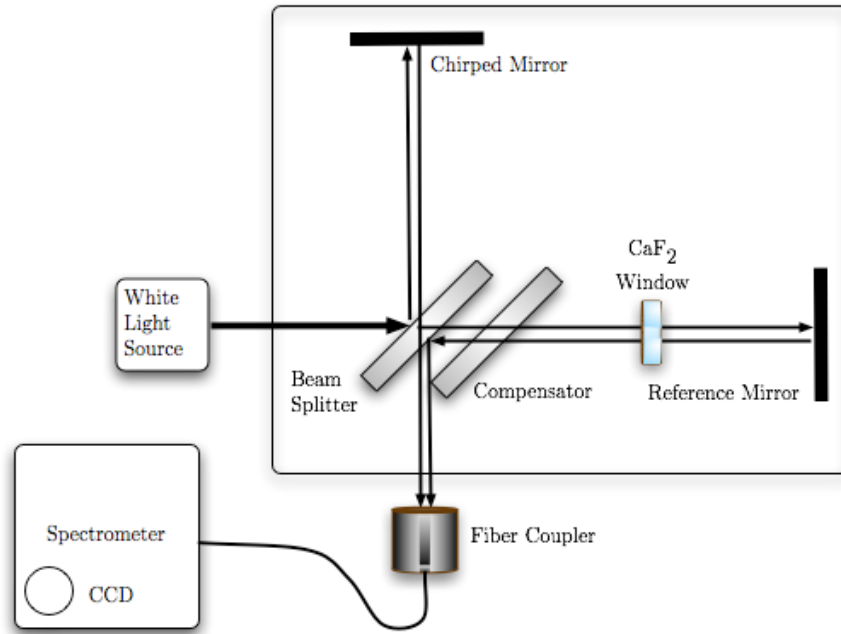
Figure 10. Michelson interferometer (MI)
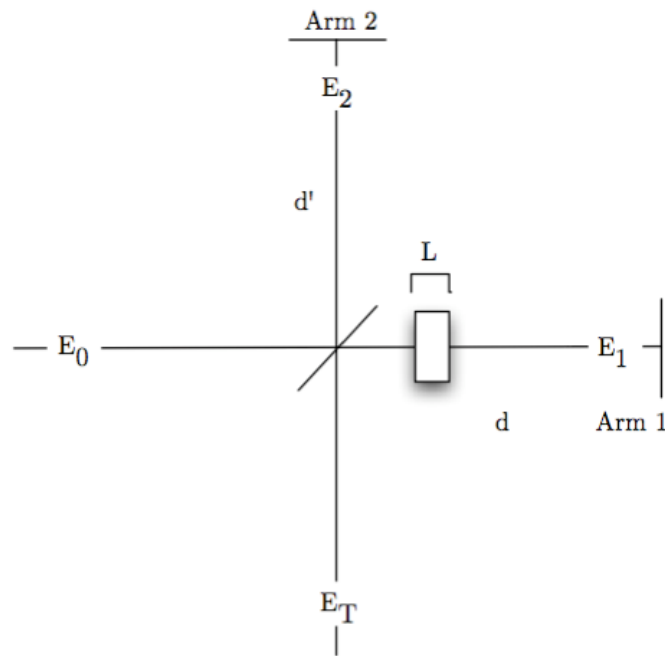
Figure 11. Simple Michelson interferometer

Figure 11 shows a simple diagram of a Michelson interferometer. A sample mirror is placed in Arm 2, and a known dispersive window is placed in Arm 1 with the reference mirror. This section explains the theory behind finding the GDD of the mirror in Arm 2.

Beginning with an electric field E_0 incident on a Michelson interferometer, the electric field is split into two beams. In Arm 1, the electric field after traversing the arm and being reflected back is

$$E_1 = \rho_1 E_0 e^{-ik_W 2L} e^{-ik2d}, \tag{2.7}$$

and the electric field in Arm 2 after reflection is

$$E_2 = \tilde{\rho}_2 E_0 e^{-ik2d'}. \tag{2.8}$$

The reflectance at each mirror is ρ_1 and $\tilde{\rho}_2$; d is the distance from the beam splitter to the first mirror; d' is the distance from the beam splitter to the second mirror; and L is the thickness of the CaF_2 window. Here, k describes propagation through air, and k_W describes propagation through the window. Combining the field in each arm yields the total electric field at the detector

$$E_T = E_1 + E_2. \tag{2.9}$$

The intensity of the combined beams is

$$I = \left| E_T \right|^2 = \left| E_1 + E_2 \right|^2 = E_1 E_1^* + E_2 E_2^* + E_2 E_1^* + E_1 E_2^*. \tag{2.10}$$

Substitute (2.7) and (2.8) into (2.10), and

$$I = \left| E_1 \right|^2 + \left| E_2 \right|^2 + \left(\tilde{\rho}_2 E_0 e^{-ik2d'} \right)\left(\rho_1^* E_0^* e^{ik_W 2L} e^{ik2d} \right) + \left(\rho_1 E_0 e^{-ik_W 2L} e^{-ik2d} \right)\left(\tilde{\rho}_2^* E_0^* e^{ik2d'} \right). \tag{2.11}$$

To include the phase change at the of the mirror, let

$$
\begin{aligned}
\rho_1^* &= \rho_1 \\
\tilde{\rho}_2 &= \left|\rho_2\right| e^{-i\phi_M} \\
\tilde{\rho}_2^* &= \left|\rho_2\right| e^{i\phi_M}
\end{aligned}
\tag{2.12}
$$

where ρ_1 is real because the reflectance of a metal mirror does not cause a

frequency dependant phase change, but the reflectance of the dispersive mirror,

$\tilde{\rho}_2$, has a complex phase component. After substituting (2.12) into (2.11), and

combining exponentials,

$$
\begin{aligned}
I &= \left|E_0\right|^2 \left|\rho_1\right|^2 + \left|E_0\right|^2 \left|\rho_2\right|^2 \\
&\quad + \left|E_0\right|^2 \left|\rho_2\right|\left|\rho_1\right| e^{-i\phi_M} e^{-ik2(d-d')} e^{ik_W 2L} \\
&\quad + \left|E_0\right|^2 \left|\rho_1\right|\left|\rho_2\right| e^{i\phi_M} e^{ik2(d-d')} e^{-ik_W 2L}
\end{aligned}
\tag{2.13}
$$

Let $\Delta = 2\left(d' - d\right)$, the difference in round-trip path length, and normalize the

incident intensity, so

$$
\frac{I}{\left|E_0\right|^2} = \left|\rho_1\right|^2 + \left|\rho_2\right|^2 + \left|\rho_1\right|\left|\rho_2\right|\left[e^{-i\left(k\Delta + \phi_M - 2k_W L\right)} + e^{i\left(k\Delta + \phi_M - 2k_W L\right)} \right].
\tag{2.14}
$$

Recall that

$$
\cos\theta = \frac{e^{i\theta} + e^{-i\theta}}{2}.
\tag{2.15}
$$

Now the normalized intensity becomes

$$
\frac{I}{\left|E_0\right|^2} = \left|\rho_1\right|^2 + \left|\rho_2\right|^2 + 2\left|\rho_1\right|\left|\rho_2\right| \cos\left(k\Delta + \phi_M - k_W 2L\right).
\tag{2.16}
$$

22

If Arm 1 is blocked, $I \propto \left|\rho_1\right|^2 \left|E_0\right|^2$, and if Arm 2 is blocked, $I \propto \left|\rho_2\right|^2 \left|E_0\right|^2$. To properly normalize the intensity of the fringes,

$$\frac{I}{\left|E_0\right|^2} \propto 2\sqrt{\rho_1}\sqrt{\rho_2} \tag{2.17}$$

where the reference is twice the square-root of the product of each arm.

Recall $k = \dfrac{2\pi n}{\lambda_0} = 2\pi\sigma n = \dfrac{\omega}{c}n$ when $\sigma = \dfrac{1}{\lambda_0}$ and $\omega = 2\pi\dfrac{c}{\lambda_0}n$. The index of refraction, n, is unity in air, but frequency dependant in general. Define the argument of the cosine in (2.16) as

$$\Psi\left(\omega\right) \equiv k\Delta + \phi_M - k_W 2L. \tag{2.18}$$

The first term of (2.18) relates to the field as it travels through air,

$$k\Delta = \frac{\omega}{c}\Delta. \tag{2.19}$$

The third term of (2.18) relates to the field as it passes through the CaF_2 window,

$$k_W = n\left(\omega\right)\frac{\omega}{c}. \tag{2.20}$$

Using a Taylor series expansion of $k_W\left(\omega\right)$ at ω_0,

$$\begin{aligned} k_W\left(\omega\right) &\cong k_W\left(\omega_0\right) + \left.\frac{dk_W}{d\omega}\right|_{\omega_0}\left(\omega - \omega_0\right) + \frac{1}{2}\left.\frac{d^2 k_W}{d\omega^2}\right|_{\omega_0}\left(\omega - \omega_0\right)^2 \\ &\cong n\left(\omega_0\right)\frac{\omega_0}{c} + \frac{1}{\nu_g}\left(\omega - \omega_0\right) + \frac{GVD_W}{2}\left(\omega - \omega_0\right)^2 \end{aligned} \tag{2.21}$$

23

where ν_g is the group velocity. The second term of (2.18) relates to the phase change at the mirror. Similar to (2.21), a Taylor series expansion of ϕ_M at ω_0 is

$$\phi_M(\omega) = \phi_M(\omega_0) + \left.\frac{d\phi_M}{d\omega}\right|_{w_0}(\omega - \omega_0) + \frac{1}{2}\left.\frac{d^2\phi_M}{d\omega^2}\right|_{w_0}(\omega - \omega_0)^2. \qquad (2.22)$$

(Note that (2.22) is identical to (6.1) in Appendix B). Combining equations (2.19), (2.21), and (2.22),

$$\Psi(\omega) = \frac{\omega}{c}\Delta$$
$$+ \phi_M(\omega_0) + \left.\frac{d\phi_M}{d\omega}\right|_{w_0}(\omega - \omega_0) + \frac{1}{2}\left.\frac{d^2\phi_M}{d\omega^2}\right|_{w_0}(\omega - \omega_0)^2 \qquad (2.23)$$
$$- 2Ln(\omega_0)\frac{\omega_0}{c} - \frac{2L}{\nu_g c}(\omega - \omega_0) - L\ GVD_W(\omega - \omega_0)^2$$

The term $\left.\dfrac{d^2\phi_M}{d\omega^2}\right|_{\omega_0}$ is the GDD of the mirror. Rearranging terms yields

$$\Psi(\omega) = \left[\frac{GDD_{\text{Mirror}}}{2} - L\ GVD_{\text{Window}}\right](\omega - \omega_0)^2$$
$$+ \left[\left.\frac{d\phi_M}{d\omega}\right|_{w_0} - \frac{2L}{\nu_g c}\right](\omega - \omega_0) \qquad (2.24)$$
$$+ \frac{\omega}{c}\Delta + \phi_M(\omega_0) - 2Ln(\omega_0)\frac{\omega_0}{c}$$

Recall that

$$(\omega - \omega_0) = (2\pi c\sigma - 2\pi c\sigma_0)$$
$$= (2\pi c)(\sigma - \sigma_0) \qquad (2.25)$$

Rewriting (2.24) in the form of a standard quadratic equation, $Ax^2 + Bx + C$,

24

$$\Psi\left(\sigma\right)=\left(2\pi c\right)^2\left[\frac{GDD_{\text{Mirror}}}{2}-L\ GVD_{\text{Window}}\right]\left(\sigma-\sigma_0\right)^2$$

$$+\left(2\pi c\right)\left[\frac{d\phi_M}{d\omega}\bigg|_{w_0}-\frac{2L}{\nu_g c}\right]\left(\sigma-\sigma_0\right) \tag{2.26}$$

$$+\frac{\omega}{c}\Delta+\phi_M\left(\omega_0\right)-2L\ n\left(\omega_0\right)\frac{\omega_0}{c}$$

The coefficient of the first quadratic term is

$$A=\left(2\pi c\right)^2\left[\frac{GDD_{\text{Mirror}}}{2}-L\ GVD_{\text{Window}}\right] \tag{2.27}$$

Rearranged,

$$GDD_{\text{Mirror}}=\frac{A}{2\left(\pi c\right)^2}+2L\ GVD_{\text{Window}} \tag{2.28}$$

The previous equation shows that the unknown group-delay dispersion of a mirror can be found using this A coefficient. The theoretical GVD of the CaF_2 window may be calculated from the Sellmeier equation with coefficients obtained from SCHOTT [19]:

$$n^2\left(\lambda\right)=1+\frac{.6188140\lambda^2}{\lambda^2-.002759866}+\frac{.4198937\lambda^2}{\lambda^2-.01061251}+\frac{3.426229\lambda^2}{\lambda^2-1068.123}. \tag{2.29}$$

Multiplying $\frac{\partial^2 n}{\partial\lambda^2}$ by twice the thickness of the window accounts for the dispersion that occurs as the beam passes through the window on its way to the mirror and again after reflection. It also converts the window's GVD with dimensions of time^2/length into GDD with dimensions of time^2. At .846 μm, 256 fs^2 is the theoretical GDD for two passes through 5 mm of CaF_2.

Curve Fitting

The curve-fit model uses (2.26)

$$y\left(\sigma\right) = \cos\left[A\left(\sigma - \sigma_0\right)^2 - P\right] + S,$$

(2.30)

where P represents a phase factor, and S is a vertical shift. Each fit yields an A coefficient which is used in (2.28) to find GDD_{Mirror} at the central delay wavelength corresponding to σ_0.

Window Effect

Curve-fitting was improved by using the CaF_2 window. The narrow stopband of chirped mirrors leaves little room for the number of interference fringes needed to apply the curve-fit model. A theoretical plot of (2.30) using (2.27) with a negative GDD mirror alone in the MI arm is shown in Figure 12a; the next plot, Figure 12b, shows the effect of placing a dispersive media in the reference arm. As the A coefficient become more negative, the number of fringes increases. One can see that the second plot gives the curve-fit more information to fit so the coefficients are more accurate.
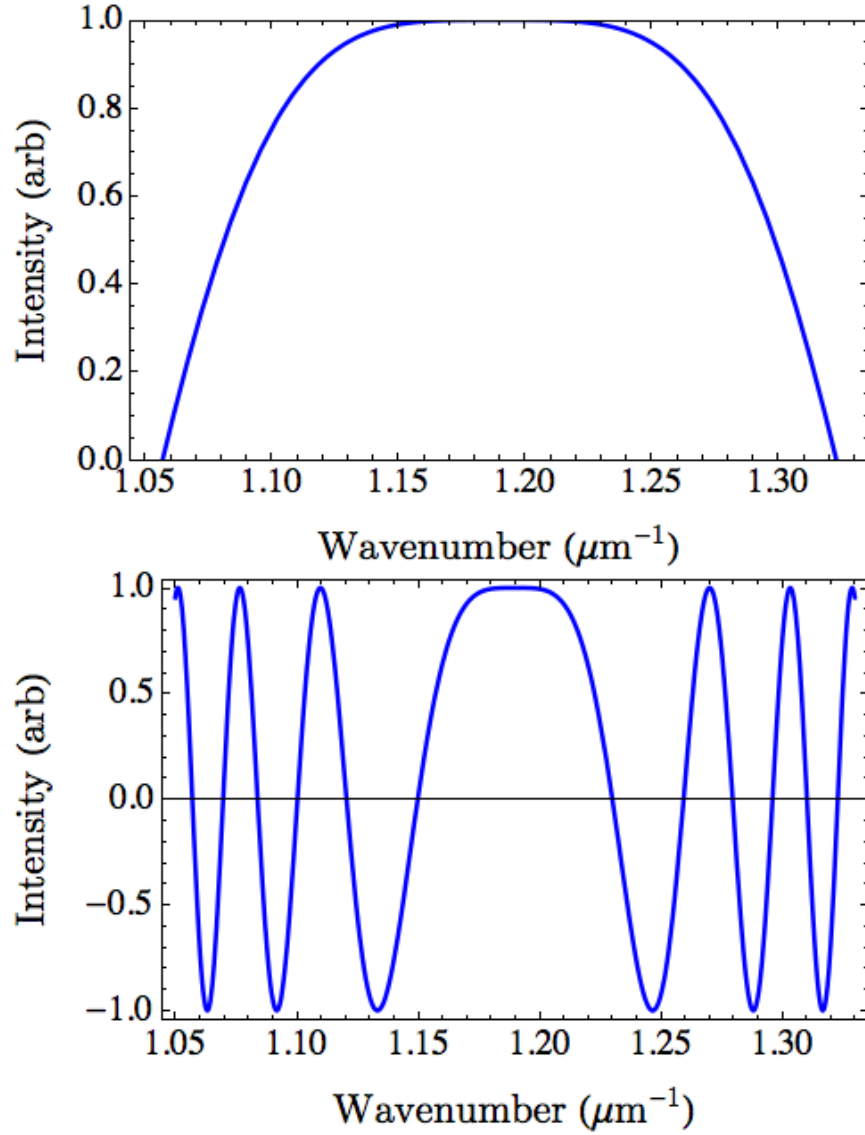
Figure 12. Theoretical fringes: a. −50 fs^2 negative GDD mirror b. −50 fs^2 negative GDD mirror with a 5 mm CaF$_2$ window in the reference arm.

FROG

In addition to finding GDD with the Michelson interferometer, a second method was employed to corroborate the results. It is a short-pulse measurement technique known as frequency-resolved optical-gating or FROG. It uses an SHG crystal and a CCD camera to give near instantaneous feedback on

wavelength, pulse width, intensity, phase vs. time, spatial profile, and spatial

chirp [20]. The Grenouille FROG, when paired with the QuickFrog software

package, measures ultra-short laser pulses directly, and provides both spatial and

temporal parameters. The Grenouille measures the actual laser pulse width and

the FWHM value for τ_p. Although it does measure spatial chirp, one drawback

to the Grenouille is that is does not provide any information on the temporal

chirp of the pulse. The basic design of a Grenouille is shown in Figure 13.

Figure 13. Grenouille FROG [20].

The Grenouille FROG was used to measure the change in pulse width after

multiple bounces between two mirrors. Using an equation similar the one used

to find the waist of a Gaussian beam, the pulse train diverges like a Gaussian

beam.

$$\tau_G = \tau_i \sqrt{1 + \left(\frac{b}{L_g}\right)^2} \tag{2.31}$$

where τ_G is the final pulse width, τ_i is the initial pulse width, and b is the number of bounces the beam makes on the mirrors. The dispersion length
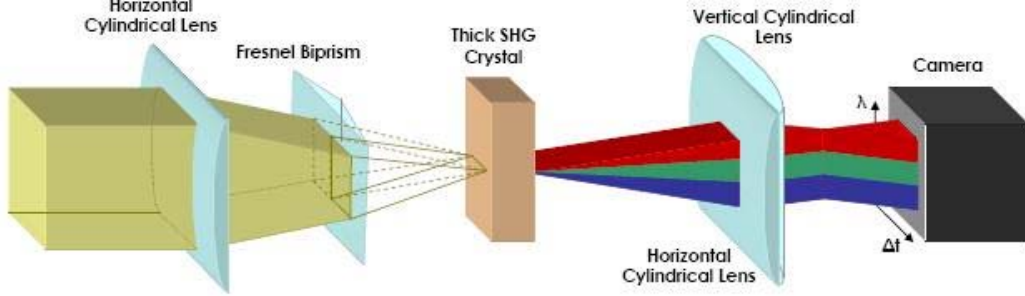
$$L_g = \frac{\tau_i^2}{2\ GDD}.$$ (2.32)

Rearranging (2.31) gives just one data point for the GDD at the wavelength of the Ti:Sapphire laser (800 nm)

$$GDD_{Mirror} = \pm \frac{\tau_i \sqrt{\tau_G^2 - \tau_i^2}}{2b}.$$ (2.33)

Cavity Dispersion

Using the mirror measurements from the MI and the FROG, it is trivial to analyze the total cavity dispersion. Knox experimentally verified that the dispersion in a cavity can simply be summed [21]. Diels supports this result, showing that linear optical elements may be characterized by a complex optical transfer function

$$\tilde{H}(\omega) = R(\omega) e^{i\Psi(\omega)},$$ (2.34)

where $R(\omega)$ is the amplitude response and $\Psi(\omega)$ is the phase delay (2.24) experienced by a spectral component of frequency ω. For a sequence of m optical elements, the total transfer function is just the product of the individual transfer functions

$$\tilde{H}(\omega) = \prod_{j=1}^m \tilde{H}_j(\omega) = \left(\prod_{j=1}^m R_j(\omega) \right) \exp\left[-i \sum_{j=1}^m \Psi_j(\omega) \right].$$ (2.35)

The exponential term contains the quadratic phase response (GDD), so each optical element in the cavity may simply be summed to determine the total GDD for the system [10].

Now that the groundwork has been laid for the Cr:LiSAF laser design, and the necessity of measuring dispersion in the laser cavity mirrors with white-light interferometry has been explained, it's time to expand on the details of the experiment.

III. Methodology

The methodology section encompasses experimental techniques used to locate fringes with the Michelson interferometer and the details of data collection and analysis.

Finding Fringes

In order to find fringes, each mirror was placed in the sample arm, while the reference arm contained a metal reference mirror and a CaF_2 window. A complex positioning process was required to locate fringes within the delay arm's limited range of movement. The device's original mirror had been attached to the front surface of the holder with a mask. In order to reproduce the location of the reflective surface, while securing the sample in the holder, the holder was suspended above the bench with two identical spacers. When the sample mirror was placed into the holder facedown, it protruded the same distance as the original mirror's thickness (Figure 14). This process meant that fringes could be found within the range of the delay arm when the sample was in the interferometer.
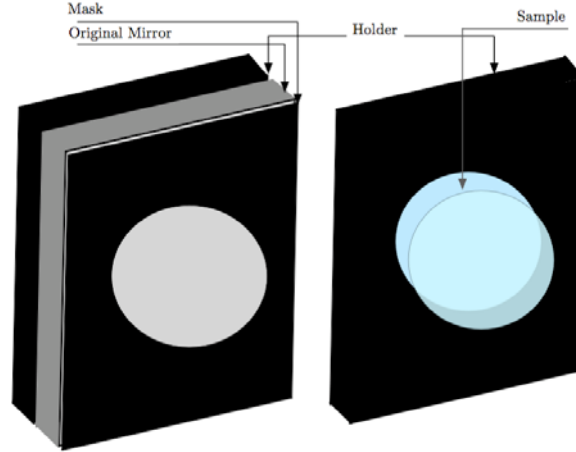
Figure 14. Sample holder

Locating fringes followed the simple process of aligning the reference mirror with the sample mirror, then adjusting the delay arm. To align the mirrors, a crosshair was placed before the beam splitter and the reference mirror was moved until both crosshair reflections overlapped. The crosshair was removed and the delay arm was scanned with small movements until fringes were located.

It was important to make small adjustments when looking for fringes. The fringes are often very thin, and the range of zero-delay very short ($\pm$ 0.01 mm). The eye cannot see them with continuous movement of the delay arm because it integrates the intensity of the fringes during their brief appearance. It is necessary to pause between each small adjustment, to give the eye an opportunity to see the fringes if they exist at that location. It is easy to make small adjustments on this interferometer because the delay arm knob is geared with a 5:1 ratio.

Once fringes are located, minute tip and tilt adjustments to the reference mirror change parallel fringes into a circular pattern. In this arrangement, the GDD of the sample mirror can be found [20]. An aperture is placed in the output beam, and stopped down so the spectrometer sees only the large center fringe.
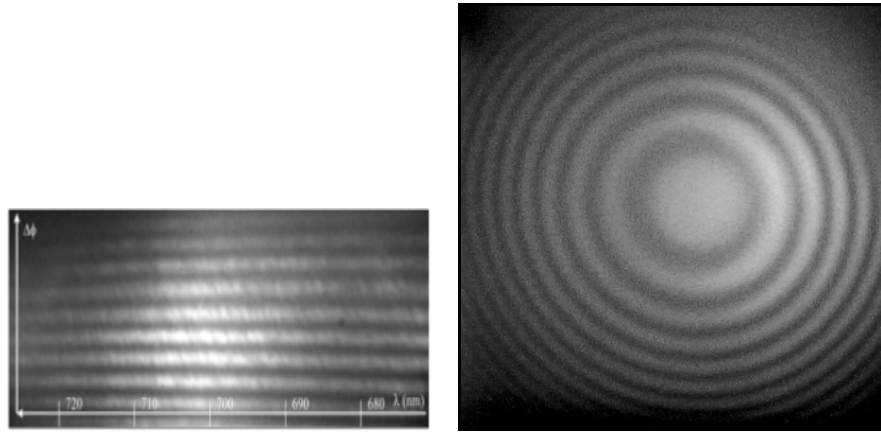
Figure 15. Example fringes a. Linear [22] b. Circular.

Data Collection

When properly adjusted into a circular fringe pattern, the range of zero-delay is no longer very short. Due to the large amount of GDD in these mirrors, fringes may be visible ± 0.15 mm on the delay arm. Scanning through this range moves the location of zero-delay across the frequencies in the white-light. Figure 16 shows zero-delay at different wavelengths for three positions of the delay arm. Most data was collected at 0.02 mm intervals over the range where fringes were visible. For each sample, two reference files are collected. The first is taken

with the sample arm blocked and the second is taken with the reference arm

blocked. The square root of the product of these two arms is used as the

reference to normalize each scan. This process is described in Equation (2.17).
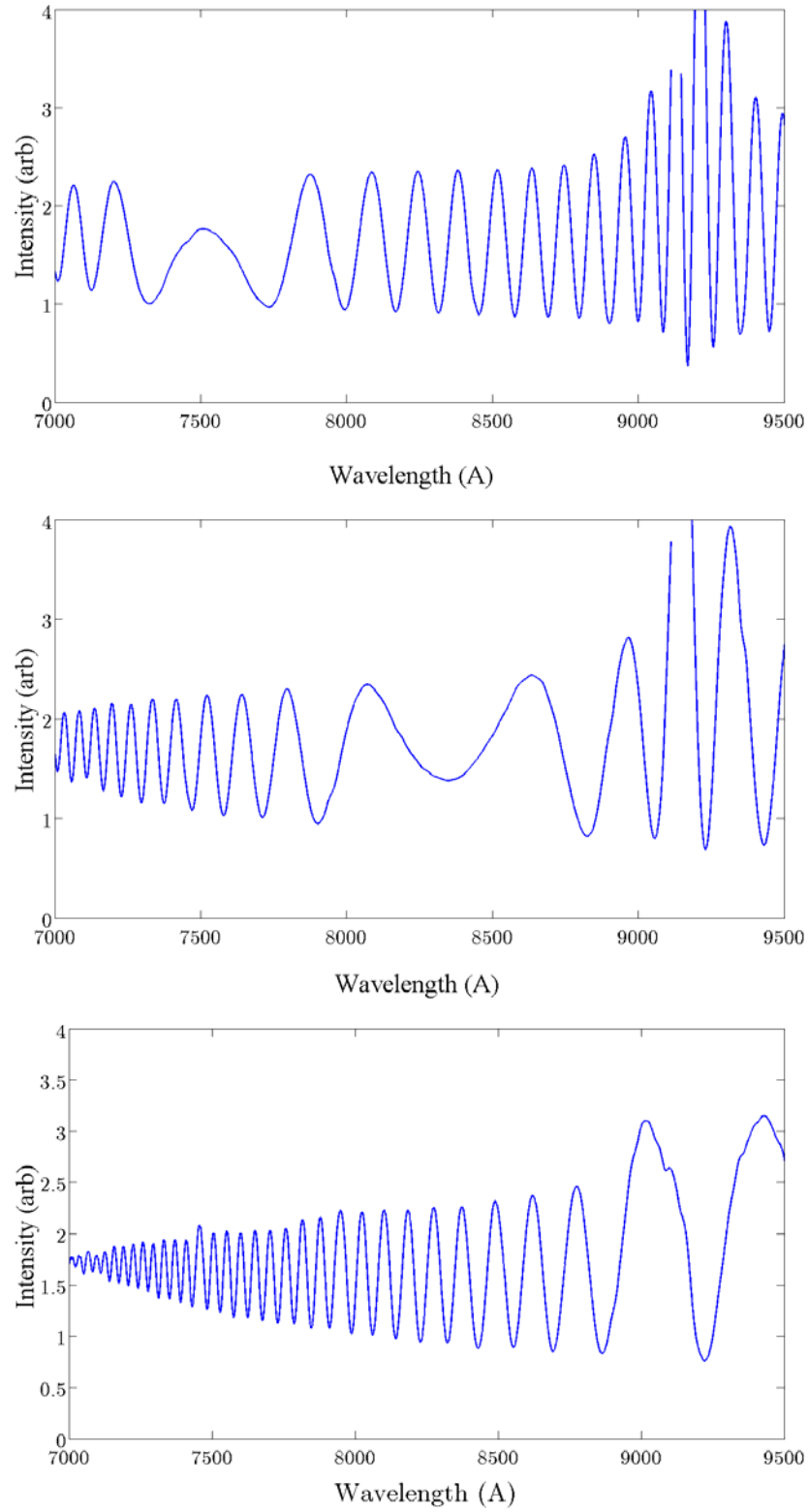
Figure 16. Example data showing the zero-delay wavelength as the delay arm is scanned

Analysis Process

It is the regions of zero-delay where the theoretical model is fit to the experimental data. The A-coefficient from the fit (2.30) is used to calculate the total GDD (2.28) for that wavelength. This curve-fitting process has been automated in MATLAB. The program is included in Appendix C. Datacruncher m-file. To summarize the procedure: the sample data is normalized using the reference data; the zero-order fringe is identified; and the model is fit to a region that includes approximately four fringes on either side of the delay (Figure 17). The A-coefficient and σ_0 are saved to an Excel workbook, where σ_0 is converted to wavelength and A's are used to find the total GDD. Since all the experimental data was collected with the CaF_2 window in the reference arm, its GDD must be removed from the total GDD to obtain the mirror's GDD. This process was discussed in the section on interference theory.

The spectrometer was configured to maximize fringe visibility without saturating the CCD detector or losing the signal entirely. On the bench, the detector and aperture were physically adjusted using near real-time feedback from the program.
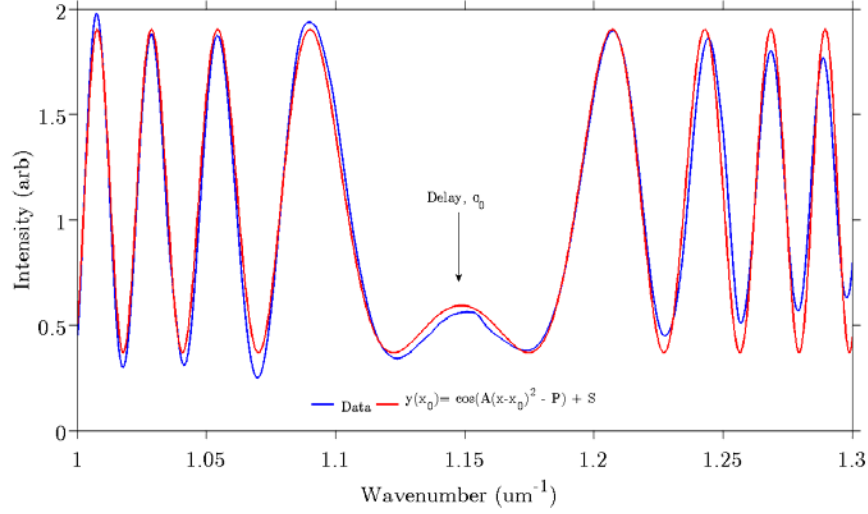
Figure 17. Example curve-fit to experimental data

FROG

A Grenouille FROG was used to confirm the MI results. Two identical

mirrors were placed so that Ti:Sapphire laser output made several bounces

before going into the Grenouille FROG. Two different sets of mirrors were each

examined with two to eight bounces (Figure 18). As a reference (τ_i), the pulses

were measured with no bounces.
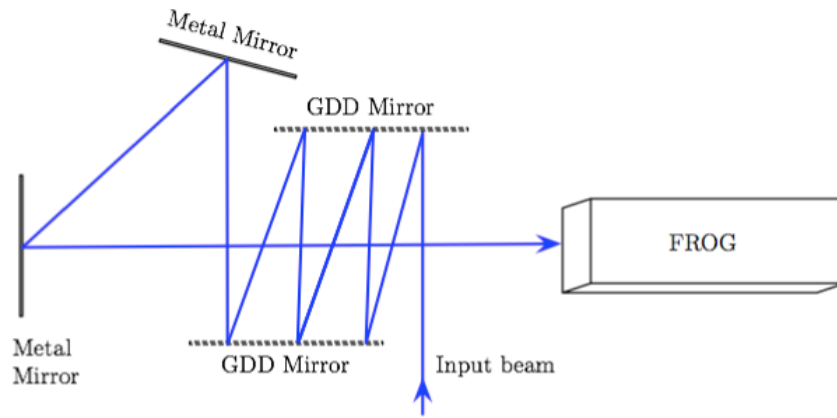
Figure 18. Six bounces before FROG

IV. Results and Analysis

This section presents the results of measuring their GDD with the Michelson interferometer and the Grenouille FROG. It addresses the offset between these results, and presents proof of modelocked operation in the Cr:LiSAF laser.

Mirrors

There were six mirrors of interest. The Newport 10Q20UF.40 Ultrafast Chirped Negative GVD mirrors are used for multiple bounces in the cavity. A photograph of a Newport mirror is shown in Figure 19. The output coupler, made by CVI (PR1-850-99-0525), is in the position opposite the Newport mirror. This mirror is slightly less reflective than the other mirrors, allowing a portion of the beam to leak out of the cavity for analysis. The two spherical mirrors were designed and manufactured specifically for this project. Their coating is engineered to transmit the pump diode wavelength, 650 nm, and reflect the 846 nm emitted by the gain media. The transmission of these mirrors is shown in Figure 20. The reflectance (1-T) is near 99.8% over a narrow region centered at 840. Since measuring curved mirrors with the Michelson interferometer is experimentally difficult, a third CVI mirror was used. This mirror has the same coating as the spherical mirrors, but it's flat. Three other mirrors, not in the laser cavity, are a New Focus 5102 NIR, Coherent GO324-005, and BATOP

SAM 262-IIIa.2. The New Focus mirrors were used as a control sample, where large positive GDD was expected. Like the CVI mirrors, the Coherent case contains two spherical mirrors and one flat mirror all with the same coating. These mirrors are available to focus the beam onto the SAM, if necessary. The SAM concept was described in Chapter II. A photograph of a SAM is shown in Figure 19b. It is made of a 0.5 in copper mount, with a 3 mm^2 mirror in the center, and it is designed to have a saturable loss of 2% absorption at 850 nm. Even though the SAM is so small in diameter with respect to the other mirrors, it was still possible to measure fringes with the MI.
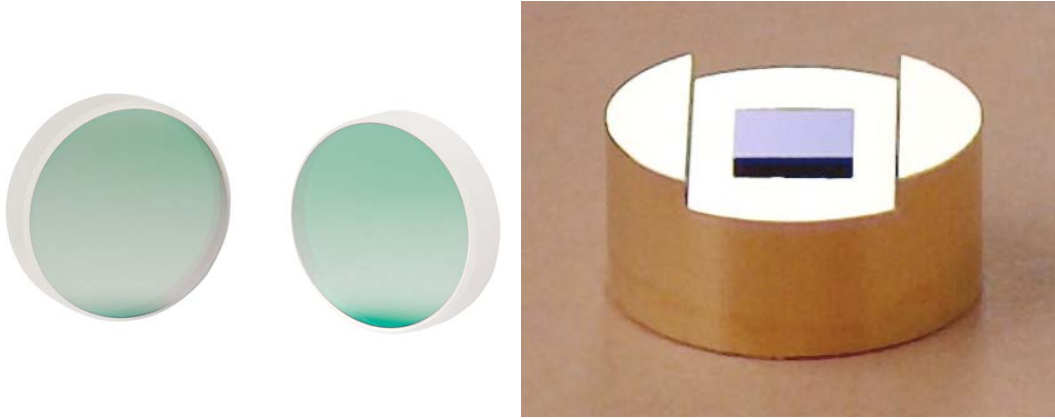
Figure 19. a. Newport mirrors (1 in) [23]. b. BATOP SAM (0.5 in) [18].
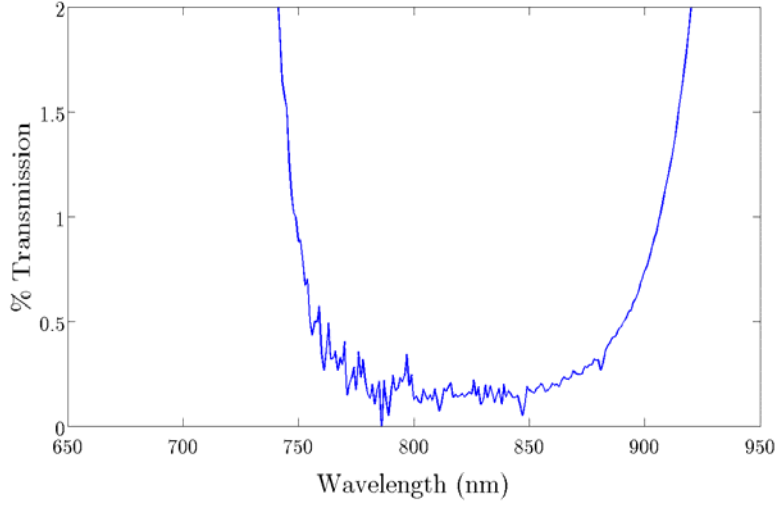
Figure 20. Transmission of CVI TNM2-800-900-0537 99.8% at 846 nm.

MI Results

Comparing the theoretical GDD for CaF$_2$ with the GDD found using this experimental fitting method validated the analysis process. At the lasing wavelength of Cr:LiSAF, the theoretical value is 256 fs^2, while the experimental measurement found it to be 288 fs^2. This is within one standard deviation of the theoretical value. Although, the difference is most likely caused by the beamsplitter and compensator in the MI, since they are each ~5 mm thick.

The experimental results for all the mirrors are presented in Figure 21. The linear fit of each data set is shown along with the R-square value indicating the goodness of each fit. The first impression of this plot is how strongly dispersive the Coherent and the New Focus mirrors are. The Coherent mirror has the lowest R-square value of all the mirrors. It is likely that the GDD of this mirror has some modulation that does not lend itself to a linear model.

40

While the New Focus, Newport, and BATOP mirrors show less modulation and have better linear fits. Another noteworthy plot is the BATOP SAM. It was not possible to obtain good curve-fits at wavelengths greater than 700 nm. The equation of the linear fit was used to estimate the GDD at 846 nm where the Cr:LiSAF lases. The same technique was used for all mirrors. Once the value of total GDD at 846 nm was identified, the experimental value of CaF_2, 288 fs^2, was subtracted as described in (2.28). Table 1 shows the GDD measured for each mirror at the lasing wavelength.
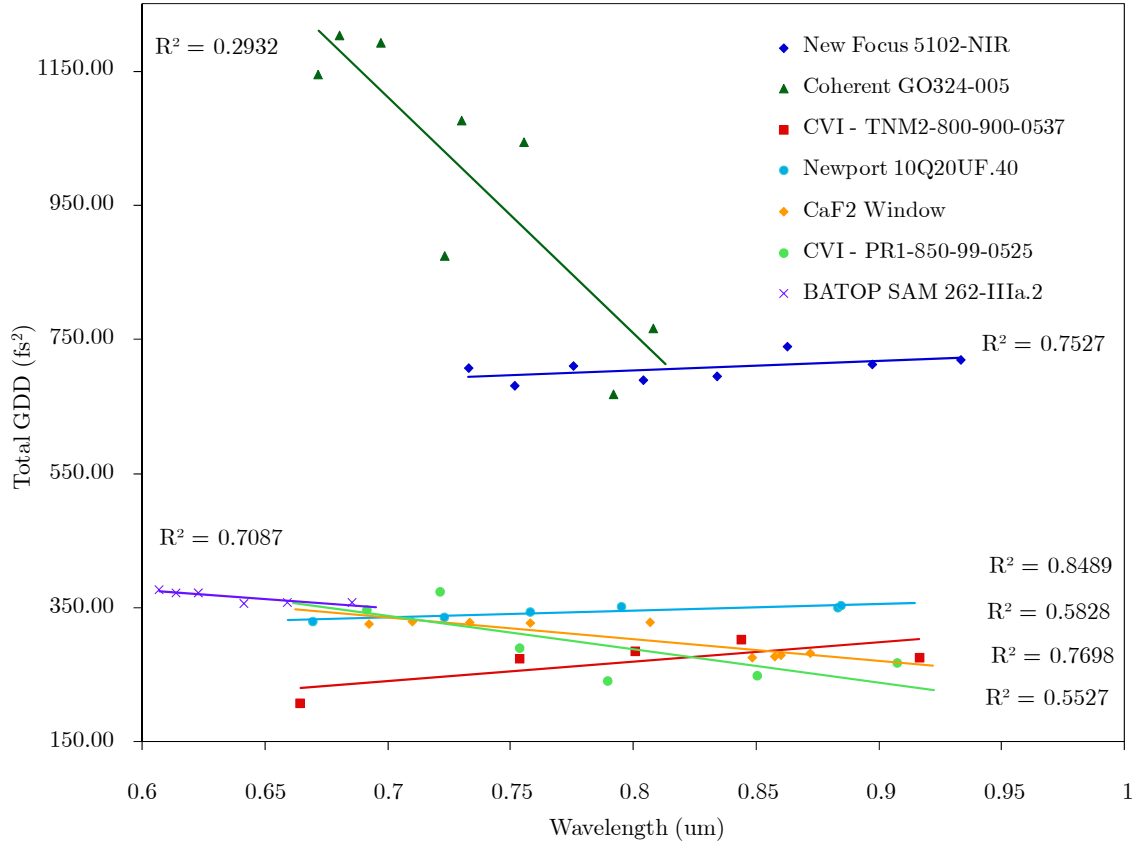
Figure 21. Data showing the R^2 values for linear fits

Table 1. GDD results from MI

Mirror	GDD at 846 nm (fs^2)
Newport 10Q20UF.40 - Ultrafast Chirped Neg GVD	60.7
New Focus 5102-NIR	420.7
Coherent GO324-005	307.7
CVI - TNM2-800-900-0537– Flat	- 6.6
CVI - PR1-850-99-0525 – Output Coupler	- 25.1
BATOP SAM 262-IIIa.2	22.54

FROG Results

The first two mirrors in Table 1 were also measured with the Grenouille FROG, and these results are shown in Table 2. The results from the FROG are closer to expected values. The second column of Table 2 shows the MI results extrapolated to 800 nm from a linear fit to each data set. The third column shows the offset between the FROG results and the MI results. The average of the differences is 120 fs^2. This value will be referred to as the FROG offset.

Table 2. GDD results from FROG

Mirror	GDD from FROG at 800 nm (fs^2)	GDD from MI at 800 nm (fs^2)	Offset (fs^2)
Newport 10Q20UF.40 Ultrafast Chirped Neg GVD	-77.45	55.9	133.35
New Focus 5102-NIR	308.41	414.27	105.86

Table 2 shows that the New Focus mirrors are much more dispersive than the Newport mirrors. It is possible to see the dispersive effect as the pulse train

mimics a diverging Gaussian beam in Figure 22. The experimental data is in blue with the theoretical beam divergence in red. This data was taken when the Ti:Sapphire laser was not very stable. Since the calculated GDD in (2.31) is very sensitive to the initial pulse width, τ_i, the reference pulse was adjusted such that the standard deviation of the results was minimized, within the normal variance of the input.

Figure 23 shows the GDD plots of these mirrors. A flat line is expected from Equation (2.31) since GDD is a constant value for each wavelength.
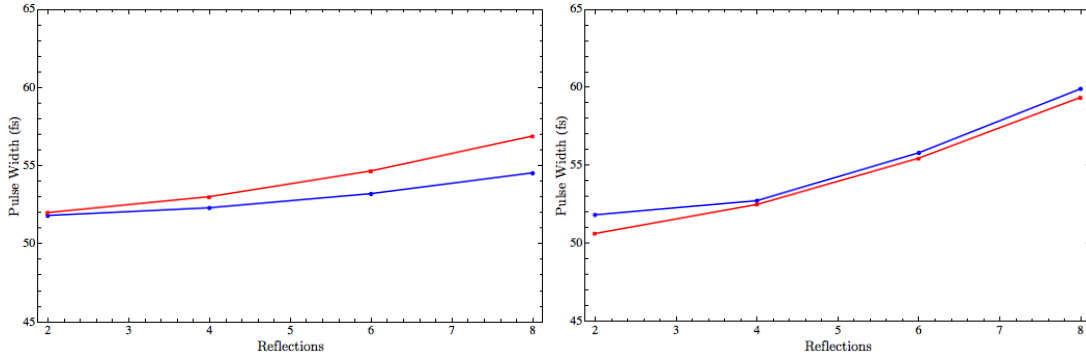
Figure 22. Beam dispersion from bounces between two mirrors a. Newport b. New Focus
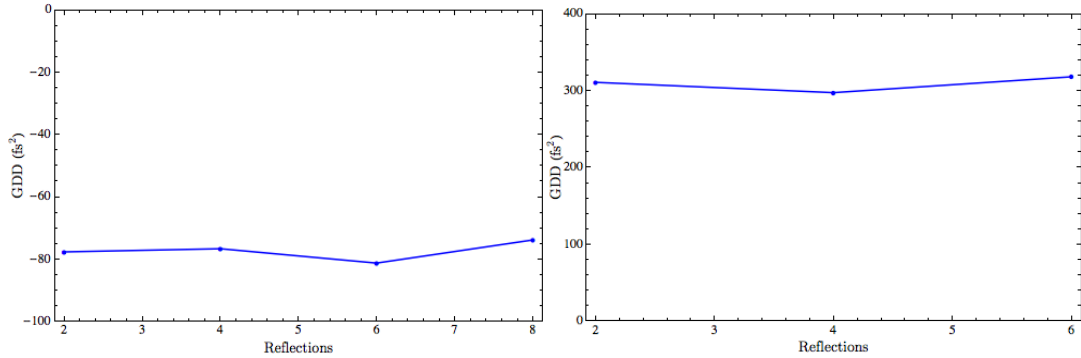
Figure 23. FROG results a. Newport b. New Focus

43

Error Analysis

Using the MI, the standard deviation of the CaF_2 measurements was 25.18 fs^2, while the standard deviation of the curve-fitting process to the experimental data was 25.45×10^{-5} μm^{-1}. Since there were no known values for the mirrors, the CaF_2 error may be extended to all the mirrors measured with the MI. Using the FROG, the standard deviation is 3.06 fs^2 for the Newport mirror, and 10.5 fs^2 for the New Focus mirror. This shows that the MI measurements were the largest source of systematic error.

After adding the CaF_2 window to the beam with multiple bounces on the Newport mirrors, and observing its effect on pulsewidth it is certain that the Newport mirrors have negative GDD. So it makes sense to consider shifting the MI results by the FROG offset, 120 fs^2. The cause of this offset is unexplained, and further analysis is necessary to understand what would cause such a significant discrepancy between the MI and the FROG measurements.

Table 3. MI results adjusted for FROG offset.

Mirror	GDD at 846 nm (fs^2)
Newport 10Q20UF.40 - Ultrafast Chirped Neg GVD	-59.3
New Focus 5102-NIR	300.7
Coherent GO324-005	187.7
CVI - TNM2-800-900-0537– Flat	-145.1
CVI - PR1-850-99-0525 – Output Coupler	- 145.1
BATOP SAM 262-IIIa.2	- 97.46

Cavity Dispersion Analysis

The dispersion of each intracavity element has been measured in isolation, and the results have been adjusted using the FROG offset (Table 3). The linear cavity in Figure 2 uses the output coupler and four CVI mirrors, two Newport mirrors, and a SAM. One may simply combine their GDD to find the dispersion of the entire resonator. Using (2.35), the sum of the crystal and the dispersive elements in the cavity is -1544.62 fs^2.

$$\underbrace{-97.46}_{\text{SAM}} + \underbrace{7 \times -145.1}_{\text{CVI}} + \underbrace{12 \times -59.3}_{\text{Newport}} + \underbrace{2 \times 75}_{\text{Cr:LiSAF}} = -1544.62 \tag{4.1}$$

It was observed that twelve bounces between the Newport mirrors were necessary to generate enough negative GDD to saturate the SAM and achieve CW modelocking. Eight bounces, resulting in -1307.54 fs^2 was not enough negative GDD for this SAM. BATOP no longer makes this product because they determined that it is not an effective device. So while it is possible to modelock the Cr:LiSAF laser using this saturable absorber mirror, the multiple bounces, and large amount of negative GDD may not be necessary with a more effective SAM. It is also important to note that if the results from the Michelson interferometer (Table 1) are not adjusted with the FROG offset, the GDD of the modelocked cavity is 855.38 fs^2. This is far from the negative value that we know is required for modelocking, and it supports the argument for using the FROG offset.

Modelocked Results

Modelocking was achieved with the cavity design described in the previous section (Figure 2). The overall CW profile is shown in Figure 24. Figure 25 zooms in to show a narrow region of the modes in the time domain. Figure 26 shows the Fourier transform into the frequency domain, where the mode spacing is 84.8 MHz, from $\nu = c/2L$. This success validates using the FROG offset, because without it, the cavity dispersion measured with the MI would be too positive to achieve modelocking.
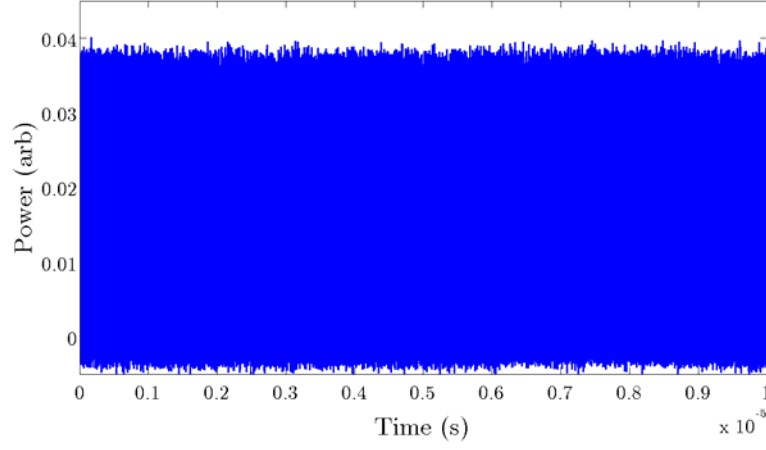
Figure 24. Q-switched modelocking in the time domain.
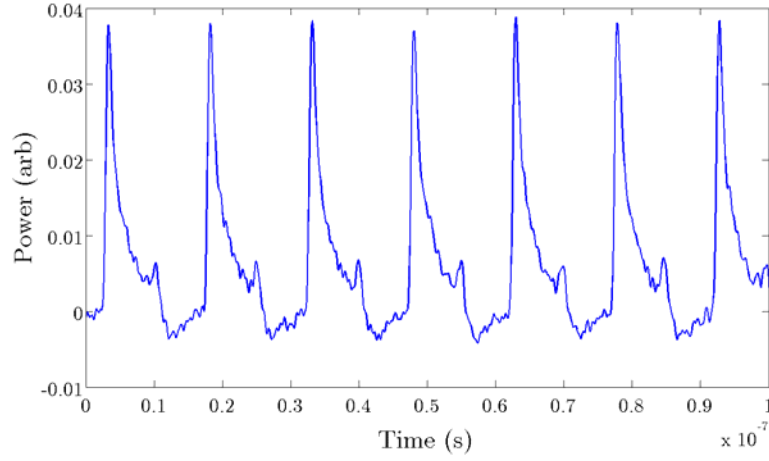
Figure 25. Zoom of time domain showing pulses.
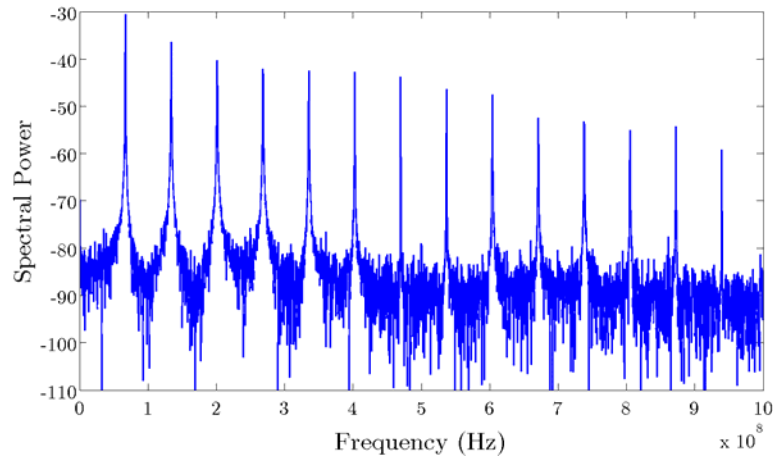
Figure 26. Frequency domain showing modes.

47

V. SUMMARY AND SUGGESTIONS

This chapter discusses the conclusions that may be drawn from the results and explains the impact of this research. It also includes suggestions for further research on this project.

Conclusions of Research

This research met the goal of measuring the dispersion in laser cavity mirrors using white light interferometry. That task was the bulk of the effort, but near the end, a cavity built with the measured mirrors was successfully modelocked. This validates the work and shows that this project is ready to move into the final phase of generating terahertz radiation.

Impact of Research

The literature review turned up papers that used interferometry to measure dispersive media like glass [24]. They mention that the theory also extends to reflective media, but none demonstrate it experimentally. So, measuring dispersive mirrors with this experiment was noteworthy.

The most significant impact of this research was the development of a new technique to measure GDD in mirrors with a narrow stop band. After an extensive literature search, no published work was found that uses a dispersive window to increase the number of spectral fringes for chirped mirrors.

Another important contribution was a careful derivation of the mathematical theory supporting this technique. Most papers gloss over the details, so this was not a trivial undertaking. It also resulted in identifying an error in a published paper [24]. This discovery is expanded on in Appendix B. Derivation of GDD Equation.

Suggestions for Further Research

The FROG offset needs further study. More mirrors should be analyzed using the FROG and MI techniques to see if the offset is consistent. The MI setup should be systematically modified to identify the source of this offset. Different dispersive windows, mirrors with wide stop-bands, alternate white-light sources are all possible changes. Overall, the technique is effective; it is just a matter of finding the right components to get measurements that are more accurate. Fortunately, the laser is not very sensitive to the magnitude of negative dispersion in the cavity, so modelocked operation was still achieved.

Measuring the cavity mirrors and modelocking the laser completes the first phase of the larger project. The second phase includes generating terahertz radiation and running on AA batteries. A photoconductive switch may be used to generate terahertz with the modelocked laser. Once the fundamental goal of generating terahertz has been accomplished, AA batteries can be used to power the pump diodes. Then the Cr:LiSAF laser will truly be a portable, affordable source of terahertz radiation.

APPENDIX A. DERIVATION OF THE NONLINEAR SCHRÖDINGER EQUATION

This derivation follows the one outlined in Boyd's <u>Nonlinear Optics</u> [25].

Consider an optical pulse traveling in the z-direction,

$$\tilde{E}\left(z,t\right)=\tilde{A}\left(z,t\right)e^{i\left(k_0 z-\omega_0 t\right)}+c.c. \tag{6.1}$$

Propagate this pulse through a dispersive, nonlinear medium. Where

$k_0 = n_{lin}\left(\omega_0\right)\omega_0 / c$. The pulse must obey the wave equation:

$$\frac{\partial^2 \tilde{E}\left(z,t\right)}{\partial z^2}-\frac{1}{c^2}\frac{\partial^2 \tilde{D}\left(z,t\right)}{\partial t^2}=0\,, \tag{6.2}$$

where $\tilde{D}$ contains both the linear and nonlinear contributions of the medium.

The Fourier transforms of $\tilde{E}\left(z,t\right)$ and $\tilde{D}\left(z,t\right)$ are:

$$\tilde{E}\left(z,t\right)=\frac{1}{2\pi}\int_{-\infty}^{\infty}E\left(z,\omega\right)e^{-i\omega t}d\omega \tag{6.3}$$

$$\tilde{D}\left(z,t\right)=\frac{1}{2\pi}\int_{-\infty}^{\infty}D\left(z,\omega\right)e^{-i\omega t}d\omega\,. \tag{6.4}$$

Remember that $E\left(z,\omega\right)$ and $D\left(z,\omega\right)$ are related by:

$$D\left(z,\omega\right)=\varepsilon\left(\omega\right)E\left(z,\omega\right). \tag{6.5}$$

Substitution of (6.3) and (6.4) into the wave equation (6.2), yields:

$$\frac{\partial^2 E\left(z,\omega\right)}{\partial z^2}+\varepsilon\left(\omega\right)\frac{\omega^2}{c^2}E\left(z,\omega\right)=0\,. \tag{6.6}$$

Focusing on the evolution of the pulse envelope, take the Fourier transform of

(6.1) and substitute the result into (6.6):

50

$$E\left(z,\omega\right)= \int_{-\infty}^{\infty} \tilde{A}\left(z,t\right)e^{i\left(k_0 z-\omega_0 t\right)}e^{i\omega t}dt$$

$$= e^{ik_o z}\int_{-\infty}^{\infty} \tilde{A}\left(z,t\right)e^{it\left(\omega-\omega_0\right)}dt \tag{6.7}$$

$$= A\left(z,\omega-\omega_0\right)e^{ik_o z}$$

where $A\left(z,\omega\right)$ is the Fourier transform of $\tilde{A}\left(z,t\right)$.

Now, the wave equation in terms of $A\left(z,\omega-\omega_0\right)$ is:

$$\frac{\partial^2}{\partial z^2}Ae^{ik_0 z}+\varepsilon\left(\omega\right)\frac{\omega^2}{c^2}Ae^{ik_0 z}=0$$

$$2ik_0 Ae^{ik_0 z}+e^{ik_0 z}\frac{\partial^2\tilde{A}}{\partial z^2}-k_0^{\,2}Ae^{ik_0 z}+\varepsilon\left(\omega\right)\frac{\omega^2}{c^2}Ae^{ik_0 z}=0 \tag{6.8}$$

Since $A\left(z,\omega-\omega_0\right)$ is a slowly varying envelope, drop the $\dfrac{\partial^2 A}{\partial z^2}$ term. From

electromagnetic theory, recall $k^2\left(\omega\right)=\varepsilon\left(\omega\right)\dfrac{\omega^2}{c^2}$. After canceling common

exponential terms,

$$\frac{\partial A\left(z,\omega-\omega_0\right)}{\partial z}ik_0 +\left(k^2-k_0^2\right)A\left(z,\omega-\omega_0\right)=0. \tag{6.9}$$

Because self-phase modulation and dispersion are considered small perturbations,

make the approximation that $k^2-k_0^{\,2}=2k_0\left(k-k_0\right)$. So,

$$\frac{\partial A\left(z,\omega-\omega_0\right)}{\partial z}i+2\left(k-k_0\right)A\left(z,\omega-\omega_0\right)=0 \tag{6.10}$$

Next, Taylor expand $k\left(\omega\right)$ about ω_0 and include the first nonlinear term:

$$k\left(\omega\right)=k_0 +n_2 I\frac{\omega_0}{c}+k'\left(\omega-\omega_0\right)+\frac{1}{2}k''\left(\omega-\omega_0\right)^2. \tag{6.11}$$

Where I is the intensity

$$I = \frac{nc}{2\pi} \left| \tilde{A}\left(z,t\right) \right|^2, \tag{6.12}$$

k' is related to the group velocity

$$k' = \left. \frac{dk\left(\omega\right)}{d\omega} \right|_{\omega=\omega_0} = \frac{1}{v_g}, \tag{6.13}$$

and k'' is the group velocity dispersion (GVD),

$$k'' = \left. \frac{d^2k\left(\omega\right)}{d\omega^2} \right|_{\omega=\omega_0} = -\frac{1}{v_g^2} \left. \frac{dv_g}{d\omega} \right|_{\omega=\omega_0} \tag{6.14}$$

Finally, make a change of variables $\Delta = \left(\omega - \omega_0\right)$, substitute (6.11) into (6.10)

and take the inverse Fourier transform, $\Im$

$$\Im\left\{ \frac{\partial A\left(z,\Delta\right)}{\partial z} - in_2 I \frac{\omega_0}{c} A\left(z,\Delta\right) - ik'\Delta A\left(z,\Delta\right) - i\frac{k''}{2}\Delta^2 A\left(z,\Delta\right) = 0 \right\} \tag{6.15}$$

From the Fourier transform tables:

$$\Im\left\{A\left(z,\Delta\right)\right\} = \tilde{A}\left(z,t\right)$$

$$\Im\left\{\Delta A\left(z,\Delta\right)\right\} = i\frac{\partial \tilde{A}\left(z,t\right)}{\partial t} \tag{6.16}$$

$$\Im\left\{\Delta^2 A\left(z,\Delta\right)\right\} = \frac{\partial^2 \tilde{A}\left(z,t\right)}{\partial t^2}$$

Substitution of these Fourier transforms yield:

$$\frac{\partial \tilde{A}\left(z,t\right)}{\partial z} - in_2 I \frac{\omega_0}{c} \tilde{A}\left(z,t\right) + k' \frac{\partial \tilde{A}\left(z,t\right)}{\partial t} + i\frac{k''}{2}\frac{\partial^2 \tilde{A}\left(z,t\right)}{\partial t^2} = 0. \tag{6.17}$$

52

Use a Galilean Boost transformation, $\tau = t - \dfrac{z}{v_g}$, to change to the reference

frame of the pulse,

$$\frac{\partial \tilde{A}\left(z,\tau\right)}{\partial z} + i\frac{k''}{2}\frac{\partial^2 \tilde{A}\left(z,\tau\right)}{\partial \tau^2} = i\frac{nn_2\omega_0}{2\pi}\left|\tilde{A}\left(z,\tau\right)\right|^2 \tilde{A}\left(z,\tau\right). \qquad (6.18)$$

Equation (6.18) is known as the nonlinear Schrödinger equation. It

describes propagation of optical pulses through dispersive media. The solutions

are solitons,

$$\tilde{A}\left(z,\tau\right) = A_0\ \mathrm{sech}\left(\frac{\tau}{\tau_0}\right)e^{-i\frac{k''}{2\tau_0^2}z}$$

$$\left|A_0\right|^2 = \frac{-2\pi k''}{nn_2\omega_0\tau_0^2} \qquad (6.19)$$

$$\tau_0 = \text{pulsewidth}$$

Note that for A_0 to be real and positive, k'' and n_2 must be of

opposite sign. Since n_2 is positive for Cr:LiSAF, k'' (GDD) must be

negative in the cavity to maintain pulsed lasing. The required

magnitude of this GDD must be determined experimentally.

APPENDIX B. DERIVATION OF GDD EQUATION

When curved fringes are observed, the curvature is quadratic [22]. The quadratic phase displacement may be written as:

$$\Delta\phi\left(\omega\right)= L\left[\frac{1}{2}\left(\omega - \omega_0\right)^2 k''\right]$$
$$= \frac{1}{2}Lk''\left(\omega - \omega_0\right)^2 \tag{8.1}$$

Where L is the length of the medium, and k'' is the group velocity dispersion of the medium at ω_0. This equation comes from a Taylor series expansion, where the first term is linear dispersion, and the second term is group-velocity dispersion. If the wavenumber, $\sigma = \frac{1}{\lambda}$, and

$$\omega = 2\pi\nu = 2\pi\frac{hc}{\lambda} = 2\pi hc\sigma\,. \tag{8.2}$$

Then substitute (8.2) into (8.1)

$$\Delta\phi\left(\omega\right)= \frac{1}{2}Lk''2^2\pi^2 h^2c^2\left(\sigma - \sigma_0\right)$$
$$= 2L\pi^2c^2k''\left(\sigma - \sigma_0\right) \tag{8.3}$$

In this situation, h is very small, and can be overlooked. Expanding (8.3),

$$\Delta\phi\left(\omega\right)= A\sigma^2 - B\sigma - C$$
$$= 2L\pi^2c^2k''\sigma^2 - 4L\pi^2c^2k''\sigma_0\sigma - 2L\pi^2c^2k''\sigma_0^2 \tag{8.4}$$

The coefficients are defined as

$$A = 2L\pi^2 c^2 k''$$
$$B = -4L\pi^2 c^2 k'' \sigma_0$$
$$C = -2L\pi^2 c^2 k'' \sigma_0^2 \ .$$

<div align="right">(8.5)</div>

Now, it's possible to find the central wavenumber, σ_0, in terms of the coefficients by noticing that B contains 2A:

$$B = -2A\sigma_0$$
$$\sigma_0 = \frac{-B}{2A} \ .$$

<div align="right">(8.6)</div>

It is known that GVD (or k'') is proportional to the dispersion in a material [11]

$$k'' = \frac{\lambda_0^3}{2\pi c^2} \frac{d^2 n}{d\lambda_0^2} \ .$$

<div align="right">(8.7)</div>

The original goal was to find the dispersion in unknown materials using the coefficients from a curve fitted to experimental data. So let's try to manipulate these equations into a useful form.

$$\frac{d^2 n}{d\lambda_0^2} = \frac{2\pi c^2}{\lambda_0^3} k'' = 2\pi c^2 k'' \sigma_0^3 = \frac{A}{\pi L} \sigma_0^3 = \frac{A}{\pi L} \frac{-B^3}{8A^3} = \frac{-B^3}{8\pi L A^2}$$

<div align="right">(8.8)</div>

Now, to find GDD, just multiply the GVD by the length of material, L:

$$\text{GDD} = k'' * L = \frac{\lambda_0^3}{2\pi c^2} \frac{d^2 n}{d\lambda_0^2} L = \frac{\lambda_0^3}{2\pi c^2} \frac{-B^3}{8\pi L A^2} L = \frac{-\left(-2A\sigma_0\right)^3}{16\pi^2 c^2 A^2 \sigma_0^3} = \frac{A}{2\left(\pi c\right)^2}$$

<div align="right">(8.9)</div>

The GDD of a mirror may be found using just the A coefficient of a quadratic equation fit to the experimental data. The central wavelength for that GDD comes from (8.6) using both the A and B coefficients. *This equation differs from the reference [24] by a factor of two.* When the

experimental result was exactly half the theoretical result of a known material, I

went to the source of the equation [22] and re-derived (8.4).

```
%%
function [datacomp] = ABDatacruncher3
datadir = '/Users/Al/Desktop/Fringe Data/20 Dec/CVI Thick';
%input is the directory where the data is located
%all files with extension *.DAT will be processed
%outputs include flist, the list if filenames in order of processing
%These variables are declared here, so they are global for this function.
xdata =0;
ydata =0;
xpos = 0;
nfiles = 1;
function button_Callback(source,eventdata)
%This function is called when the continue button is called
%Rescale data set to match selected 'zoomed in' area
xpos = xlim;
close(fig);
xpos1 = floor(xpos(1));
xpos2 = floor(xpos(2));
xdata = 10000./xdata(xpos1:xpos2);
ydata = smooth(ydata(xpos1:xpos2),'rlowess',.01);
%This section finds a guess at the central wavenumber by looking
%for the maximum of the fourier domain versus the new variable x2.
%x2 is a new variable that goes as x^2
%after scaling the x2fft, the new y's are resampled
x2 = (xdata-centerpos).^2;
x2max = max(x2);
x2min = min(x2);
x2new = x2min+(0:(length(x2)-1))*(x2max-x2min)/(length(x2)-1);
x2fft = (0:((length(x2)/2)-1))/(x2max-x2min);
```

```
y2 = smooth(interp1(x2,ydata,x2new),'rlowess',.1);
y2fft = abs(fft(y2));
y2fft = y2fft(1:length(x2fft));
%plot(x2fft,y2fft);
[c,iy2max]= max(y2fft(3:length(x2fft)));
fguess = 2*pi*x2fft(iy2max+2);
end

function ok_Callback(source,eventdata)
%This function is called when the OK butten is pushed.
%The structure datacomp is saved to the current directory as a workplace file.
save datacomp.mat datacomp;
nfiles = nfiles+1;
close(fig);
end

function redo_Callback(source,eventdata)
%This function is called when the redo button is pushed.  It simply
%starts the data analysis over with the current file.
close(fig);
end

function txt = myupdatefcn(empt,event_obj)
%function called when the plot is clicked
pos = get(event_obj,'Position');
centerpos = 10000/xdata(pos(1));
txt = {['Wavelength: ',num2str(xdata(pos(1)))]};
line([pos(1) pos(1)],[0 3]);
end

%This is the beginning of the function
%It reads the list of data files and the reference file.
%Then the reference file is smoothed.  Before entering the major while loop.
datalist = dir(fullfile(datadir,'*.DAT'));
reflist = dir(fullfile(datadir,'*.ref'));
```

```matlab
refinput = importdata(fullfile(datadir,reflist(1).name));
refinput = refinput.data;
refdata = smooth(refinput(:,2),.01,'rlowess');
while(nfiles <= length(datalist))
%Read in the data file, normalize it with the ref and smooth data.
datainput = importdata(fullfile(datadir,datalist(nfiles).name));
datainput = datainput.data;
xdata = datainput(:,1);
ydata = datainput(:,2)./refdata;
ydata=smooth(ydata,.01,'rlowess');
%Generates data plot and turns on the cursormode
fig = figure('Toolbar','figure');
plot(ydata);
ylim([0 4]);
zoom on;
dcm_obj = datacursormode(fig);
set(dcm_obj,'UpdateFcn',@myupdatefcn);
% Help directions printed to screen
text(0,2.9,'Zoom to select range. Cursor to select center','FontSize',12);
text(0,2.6,'Then press continue','FontSize',12);
%Generate continue push button and wait for user to to push continue
pbh = uicontrol(fig,'Style','pushbutton','String','Continue','Position',[10 10 60
40],'Callback',{@button_Callback});
uicontrol(pbh);
uiwait(fig);
%call nonlinear fit using the function fringe.  fguess and the selected
%center point are input into the guess.
[betahat,resid,J] = nlinfit(xdata,ydata,'fringe',[fguess,centerpos,3,1,1]);
%The fitting routine could be called a second, or third time; however
%it did not seem to help.
%[betahat,resid,J] = nlinfit(xdata,ydata,'fringe',betahat);
```

```matlab
%betahat
%betahat,resid,J] = nlinfit(xdata,ydata,'fringe',betahat);
%betahat
%nlparci returns the 95% confidence interval for the fitted parameters
betaci = nlparci(betahat,resid,J);
A(nfiles) = betahat(1);
sigmaA(nfiles) = abs(betaci(1,1)-betaci(1,2))/2;
sigma0(nfiles) = betahat(2);
sigma0sigma(nfiles)=abs(betaci(2,1)-betaci(2,2))/2;
yfit = fringe(betahat,xdata);
%create arrays of data and store in structure datacomp
flist{nfiles} = datalist(nfiles).name;
datalist(nfiles).name
datacomp(nfiles) = struct('filename',datalist(nfiles).name,
'Acoefficient',A(nfiles),'sigmaA',sigmaA(nfiles),'sigma0',sigma0(nfiles),'sigma0sigm
a',sigma0sigma(nfiles));
plot(xdata, ydata,'*',xdata,yfit,'+');
%generate ok and redo push buttons
pbok = uicontrol(fig,'Style','pushbutton','String','Ok','Position',[10 10 60
40],'Callback',{@ok_Callback});
uicontrol(pbok);
pbredo = uicontrol(fig,'Style','pushbutton','String','Retry','Position',[10 50 60
40],'Callback',{@redo_Callback});
uicontrol(pbredo);
xlabel('Wavenumber (1/microns)');
ylabel('Fringe Amplitude (normalized)');
title('Fitting Fringe');
legend('data', 'Fringe Fit');
uiwait(fig);
end %while loop end
end %function end
```

```
function yhat = fringe(beta,x)
A = beta(1);
b = beta(2);
c = beta(3);
d = beta(4);
f = beta(5);
yhat = f+d*cos(A*(x-b).^2+c);
end
```

BIBLIOGRAPHY

1. Jones, D. A. (2007). *Portable diode-pumped femtosecond lasers.* MS Thesis, AFIT/ENP/GAP/07-04. Graduate School of Engineering and Management, Air Force Institute of Technology (AU), Wright-Patterson AFB OH, March 2007.uiol,

2. Binns, C. Shadowy T-rays: Hunting tumors and exploring the universe. Available at *http://www.livescience.com/technology/060728_t-rays.html*, 2006.

3. Krueger, A., Victor, D., & Feru, P. TUNABLE SOURCES: Dispersion compensation sharpens multiphoton microscopy. *Laser Focus World*, 43, 2007.

4. Dymott, M. J., Ferguson, A. I. Self-mode-locked diode-pumped Cr:LiSAF laser. *Optics Letters*, 19, 1988, 1994.

5. Valentine, G. J., Hopkins, J. M., Loza-Alvarez, P., Kennedy, G. T., Sibbett, W., Burns, D. Ultralow-pump-threshold, femtosecond Cr^{3+}:LiSrAlF$_6$ laser pumped by a single narrow-stripe AlGaInP laser diode. *Optics Letters*, 22, 1639, 1997.

6. Samad, R. E., Baldochi, S. L., Eduardo, G., Nogueira, C., Vieira, N. D. 30W Cr:LiSrAlF$_6$ flashlamp-pumped pulsed laser. *Optics Letters*, 32, 50-52, 2007.

7. Verdeyen, J. T. *Laser Electronics (3rd ed.).* Upper Saddle River: Prentice Hall, 2000.

8. Diddams, S. A., Diels, J.-C., Dispersion measurements with white-light interferometry. *J. Opt. Soc. Am. B*, 13, 1120, 1996.

9. Van Enge, A. G., Diddams, S. A., Clement, T. S., Dispersion measurements of water with white-light interferometry. *Applied Optics*, 37, 5679, (1988).

10. Diels, J.-C., & Wolfgang, R., In Liao P. F., Kelley P. L. and Kaminow I. (Eds.), *Ultrashort laser pulse phenomena (1st ed.)*. San Diego, California, 92101: Academic Press, 1996.

11. VLOC. Cr:LiSAF, LiSGaF and LiCaF physical and optical properties. Product information guide, October 2006. Available at *http://www.vloc.com/PDFs/OtherGainMaterials/Cr LiSAF LiSGaF LiCAF.pdf*, 2007.

12. Walmsley, I., Waxer, L., & Dorrer, C. The role of dispersion in ultra fast optics. *Review of Scientific Instruments*, 72(1), 1, 2001.

13. Saleh, B. E. A., Teich, M. C. In Saleh B. E. A. (Ed.), *Fundamentals of Photonics (Second Edition ed.)*. Hoboken, New Jersey: John Wiley & Sons, Inc, 2007.

14. Paschotta, R. Encyclopedia of Laser Physics and Technology - Chirped mirrors. Available at *http://www.rp-photonics.com*, 2007.

15. Matsuda, I., Misawa, K., & Lang, R. Femtosecond chirp-variable apparatus using a chirped mirror pair for quantum coherent control. *Optics Communications*, 239(1-3), 181-186, 2004.

16. Wikipedia contributors. Kerr-lens effect. Retrieved 16 October 2007.

17. BATOP Optoelectronics, Inc. How does a SAM work? Available at *http://www.batop.de/informations/SAM_infos.html*, 2008.

18. Hecht, E. *Optics (4th ed.)*. San Francisco: Pearson Education, 2002.

19. SCHOTT. Available at
    *http://www.schott.com/lithotec/english/download/caf2_february_ 2007_final
    .pdf*, 2007.

20. Swamp Optics. GRENOUILLE model 8-50 User's guide. Atlanta, GA 30339.

21. Knox, W., Pearson, N., Li, K., & Hirlimann, C. Interferometric
    measurements of femtosecond group delay in optical components. *Optics
    Letters*, 13, 574, 1988.

22. Parys, B., Allard, J., Morris, D., Pepin, C., Houde, D., & Cornet, A.
    Assessment of the spectral interference method applied to the stretching
    measurement of diffused laser pulses. *J. Opt. A.*, 7, 249, 2005

23. Newport. Available at *http://www.newport.com/Ultrafast-Laser-Chirped-
    Mirrors/543092/1033/catalog.aspx#*, 2007.

24. Debnath, S. K., Viswanathan, N. K., & Kothiyal, M. P. Spectrally resolved
    phase-shifting interferometry for accurate group-velocity dispersion
    measurements. *Optics Letters*, 31, 3098-3100, 2006.

25. Boyd, R. W. *Nonlinear Optics (1st ed.)*. Boston: Academic Press, 1992.

REPORT DOCUMENTATION PAGE

The public reporting burden for this collection of information is estimated to average 1 hour per response, including the time for reviewing instructions, searching existing data sources, gathering and maintaining the data needed, and completing and reviewing the collection of information. Send comments regarding this burden estimate or any other aspect of this collection of information, including suggestions for reducing the burden, to the Department of Defense, Executive Services and Communications Directorate (0704-0188). Respondents should be aware that notwithstanding any other provision of law, no person shall be subject to any penalty for failing to comply with a collection of information if it does not display a currently valid OMB control number.

PLEASE DO NOT RETURN YOUR FORM TO THE ABOVE ORGANIZATION.

1. REPORT DATE *(DD-MM-YYYY)*	2. REPORT TYPE	3. DATES COVERED *(From - To)*

4. TITLE AND SUBTITLE

5a. CONTRACT NUMBER

5b. GRANT NUMBER

5c. PROGRAM ELEMENT NUMBER

6. AUTHOR(S)

5d. PROJECT NUMBER

5e. TASK NUMBER

5f. WORK UNIT NUMBER

7. PERFORMING ORGANIZATION NAME(S) AND ADDRESS(ES)

8. PERFORMING ORGANIZATION REPORT NUMBER

9. SPONSORING/MONITORING AGENCY NAME(S) AND ADDRESS(ES)

10. SPONSOR/MONITOR'S ACRONYM(S)

11. SPONSOR/MONITOR'S REPORT NUMBER(S)

12. DISTRIBUTION/AVAILABILITY STATEMENT

13. SUPPLEMENTARY NOTES

14. ABSTRACT

15. SUBJECT TERMS

16. SECURITY CLASSIFICATION OF:			17. LIMITATION OF ABSTRACT	18. NUMBER OF PAGES	19a. NAME OF RESPONSIBLE PERSON
a. REPORT	b. ABSTRACT	c. THIS PAGE			
					19b. TELEPHONE NUMBER *(Include area code)*